5.11 Seismic Response of Cable Stayed bridges

1) Dynamic Characteristics of Cable Stayed bridges Based on Forced Excitation Tests

Cable stayed bridges are complex structures consisting of various structural components with different stiffness and damping characteristics. They are more flexible than girder bridges, and precise structural analysis is required in seismic design. In the seismic design of cable stayed bridges, it is essential to accurately evaluate the natural periods, natural mode shapes and damping characteristics. To verify the validity of the seismic design, field forced excitation tests have been conducted for cable stayed bridges. Because most tests were conducted to clarify the aerodynamic stability, bridges were generally excited in the vertical direction. Dynamic properties of vertical flexural oscillations and torsional oscillations are key issues in the wind resistant design. In some cases, however, excitation was conducted for flexural oscillations in the transverse direction. Some typical results are presented in the following (Kawashima, Unjoh and Tsunomoto 1991).

a) Onomiti Bridge

Onomiti Bridge is a part of the Honshu-Shikoku Bridge, which consists of a three span continuous steel girder deck and two towers as shown in Fig. 5.109. The center span is 215 m long and the total bridge length is 386 m. A series of forced excitation tests was conducted to excite vertical flexural oscillations and torsional oscillations using rotating eccentric mass shakers. Fig.5.110 shows mode shapes determined by the tests. Mode shapes computed by a linear flame analysis are presented in Fig. 5.111 for comparison. The computed mode shapes agree well with the measured ones. Table 5.3 shows comparison of the natural frequencies between the measured and the computed. Agreement of the natural frequency is satisfactory.

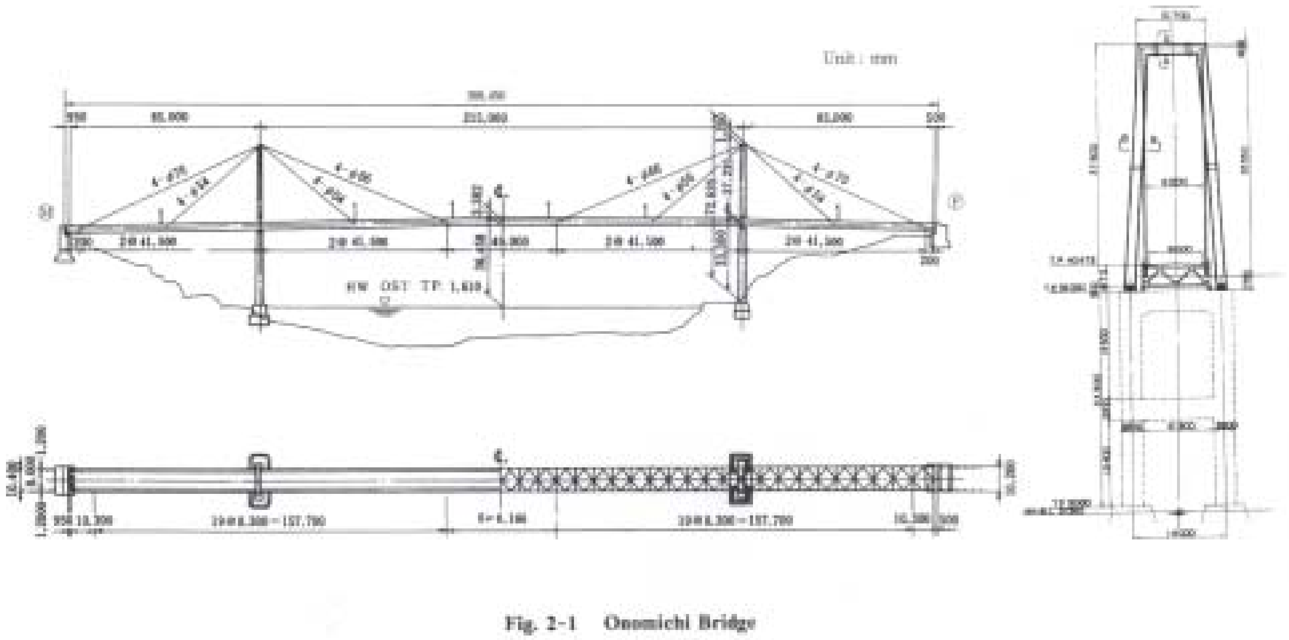

Fig. 5.109 Onomichi Bridge

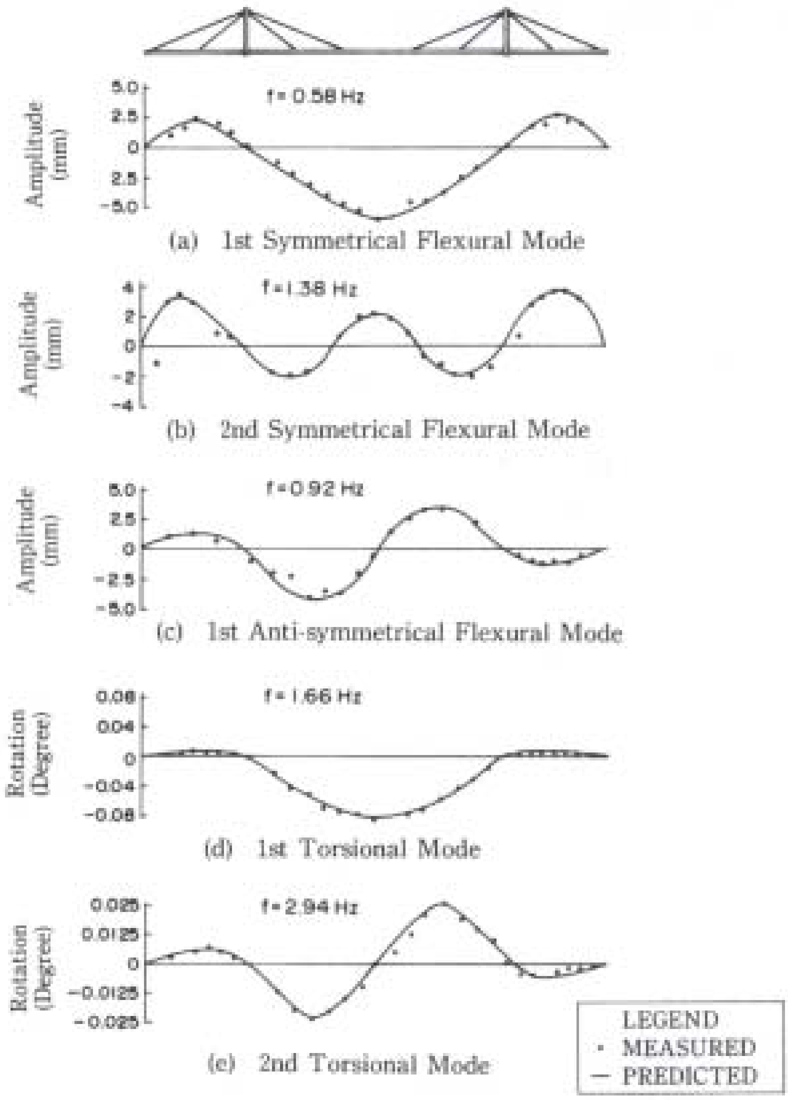

Fig. 5.110 Correlation of Computed Mode Shapes to the Measured Based on Forced Excitation Test (Onomichi Bridge)

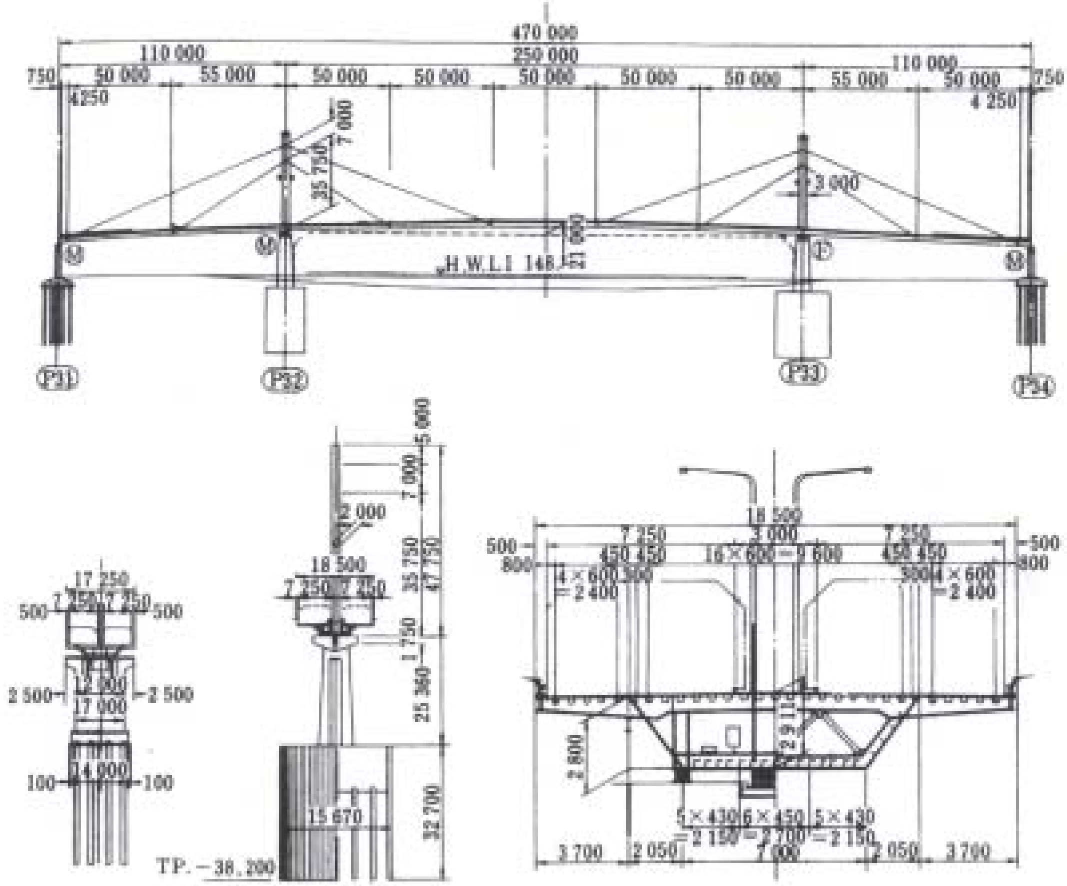

Fig. 5.111 Suehiro Bridge

Damping ratios ξ were evaluated from the logarithmic damping ratio δ of a free decay of the flexural oscillations as

$$\delta = \frac{2\pi\xi}{\sqrt{1-\xi^2}} = \log_e \frac{a_m}{a_{m+1}} \tag{5.61}$$

where a_m and a_{m+1} represent the amplitude at m-th and (m+1)th peak amplitudes, respectively, of a free oscillation. The damping ratios evaluated by Eq. (5.61) in the vertical flexural and torsional oscillations are also presented in Table 5.3. Damping ratios are less than 0.01 for both the flexural and torsinal oscillations.

Table 5.3 Natural Frequencies and Damping Ratios of Onomichi Bridge

Mode Shapes		Mode No.	Natural Frequencies (Hz)		Damping Ratio
			Measured	Computed	
Vertical Flexure	Symmetric	1st	0.58	0.581	0.008
		2nd	1.38	1.385	-
	Anti-Symmetric	1st	0.92	0.914	0.0072
		2nd	1.62	1.562	-
Torsion	Symmetric	1st	1.66	1.706	0.0056
	Anti-Symmetric	2nd	2.94	3.055	0.0048

b) Suehiro Bridge

Suehiro Bridge is a three span continuous steel box girder bridge supported by two single towers as shown in Fig. 5.111. A force excitation test was conducted for vertical flexural and torsional oscillations. Fig. 5.112 shows a comparison of the mode shapes between the measured and the computed by a linear discrete flame analysis. The computed mode shapes are very close with the measured mode shapes. Table 5.4 shows a comparison of measured and computed natural frequencies as well as measured damping ratios.

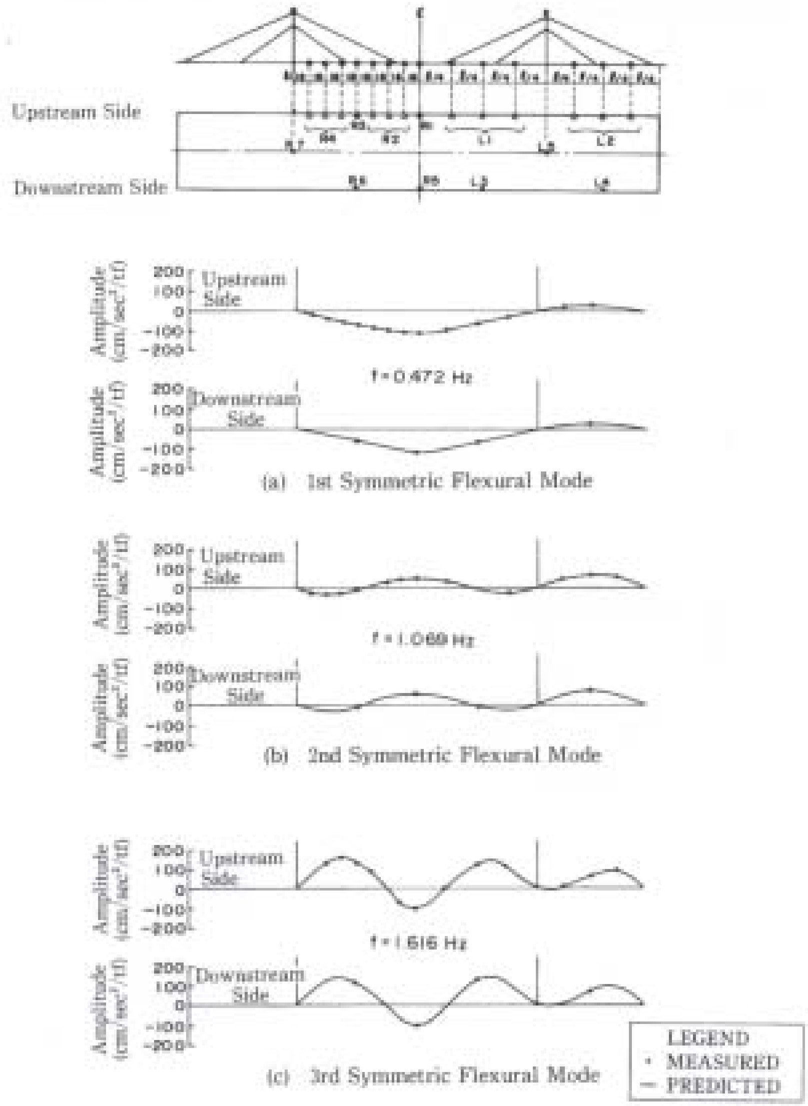

Fig. 5.112 Correlation of Computed Mode Shapes to the Measured (Suehiro Bridge)

The damping ratios are evaluated by (1) decay of the free oscillations, (2) half-power method using resonance curves, and (3) half-power method using frequency response functions obtained based on micro tremor. In the half-power method, a damping ratio ξ is evaluated as

$$\xi = \frac{f_2 - f_1}{2 f_0} \tag{5.62}$$

where f_0: frequency corresponding to the peak response amplitude a_{max} during a forced excitation, and f_1 and f_2: smaller and larger frequencies corresponding to the amplitude equal to $a_{max} / \sqrt{2}$. Since amplitudes of oscillations in micro tremor are very small, the damping ratios derived from micro tremor reflects energy dissipation of the bridge during oscillations with very small amplitudes.

It is interesting to compare the damping ratios which are obtained by the different methods for the same mode shape. Although damping ratios evaluated by micro tremor tends to yield smaller values than those evaluated by the decay of free oscillations, this is not the case in this bridge. The damping ratios evaluated by the three methods are all smaller than 0.01.

Table 5.4 Natural Frequencies and Damping Ratios of Suehiro Bridge

Mode Shapes			Natural Frequencies (Hz)		Damping Ratios		
			Measured	Computed	Decay of Free Oscillations	Resonance Curves	Micro Tremor
Flexure	Symmetric	1st	0.472	0.468	0.0049	-	0.0068
		2nd	1.069	1.116	0.0286	0.0021	0.0025
		3rd	1.616	1.722	0.0019	0.0017	0.0030
	Anti-Symmetric	1st	0.712	0.746	0.0029	0.0022	0.0040
		2nd	1.264	1.334	0.0025	0.0031	0.0022
		3rd	2.094	2.150	-	0.0077	-
Torsion	Symmetric	1st	1.446	1.537	0.0025	0.0039	0.0026
		2nd	4.444	4.487	-	0.0127	-
		3rd	6.712	6.983	-	0.0061	-
	Anti-Symmetric	1st	2.888	3.020	0.0089	0.0043	0.0018

c) Yamato-gawa Bridge

Yamato-gawa Bridge is a part of the Osaka Bay Circulating Highway, and it is a three span continuous steel deck girder supported by two single towers as shown in Fig. 5.113. The center span is 355 m long. The bridge was excited for vertical flexural and torsional oscillations by pulling up and down a heavy masses at varying a location on the deck. Fig. 5.114 shows that computed mode shapes agree well with the measured mode shapes. Table 5.5 shows the measures and computed natural frequencies, and measured damping ratios. Of particular interest is the damping ratios. Similar to Suehiro Bridge, damping ratios were evaluated by (1) resonant curves using the half-power method and (2) micro tremor using the half-power method. It is noted that the damping ratios evaluated by the two methods are nearly the same for the same modes. The damping ratios depend on mode shapes, and they are generally less than 0.01.

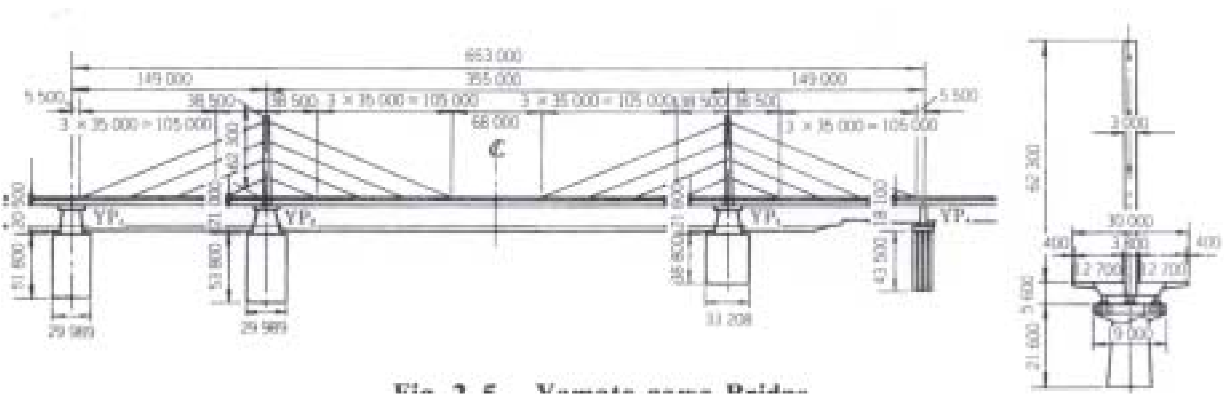

Fig. 5.113 Yamato-gawa Bridge

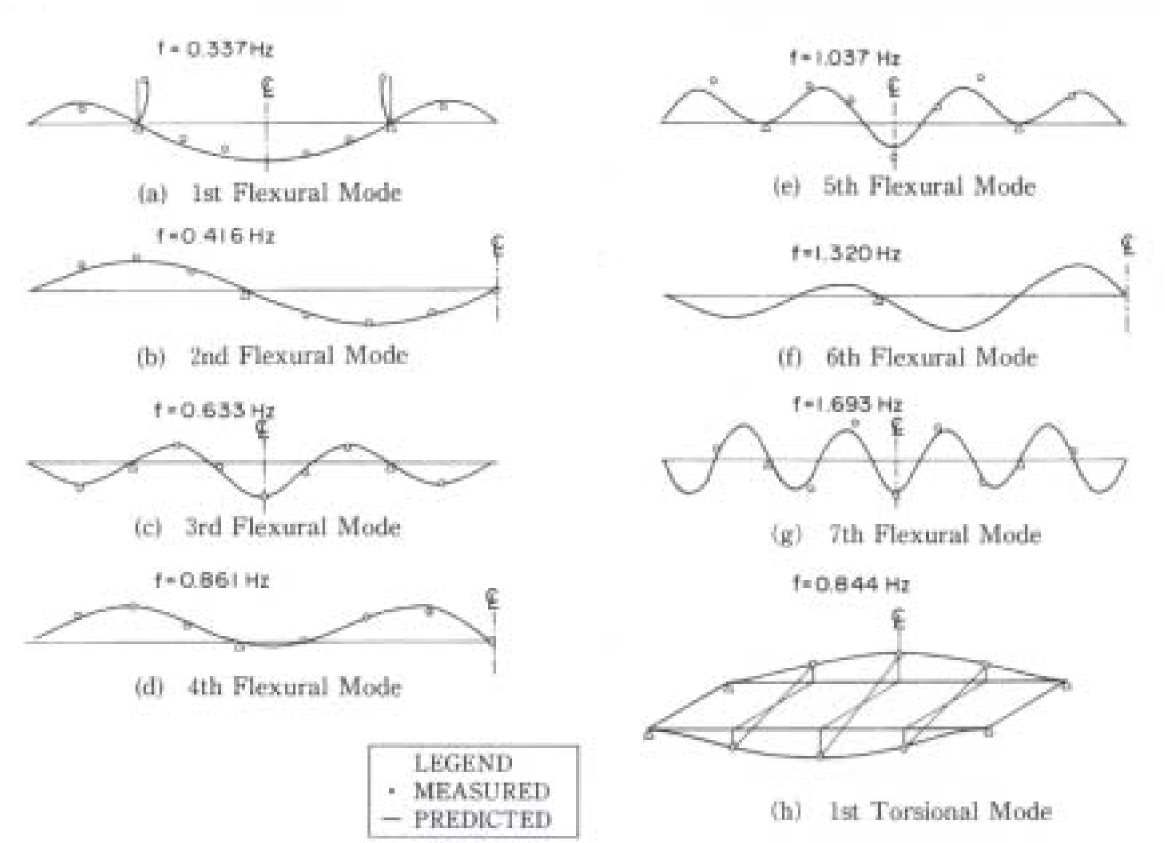

Fig. 5.114 Correlation of Computed Mode Shapes to the Measured (Yamato-gawa Bridge)

Table 5.5 Natural Frequencies and Damping Ratios of Yamato-gawa Bridge

Mode Shapes		Natural Frequencies (Hz)		Damping Ratios	
		Measured	Computed	Resonance Curve	Micro Tremor
Flexure	1st	0.337	0.319	0.0035-0.0038	0081-0.0087
	2nd	0.416	0.372	0.0048-0.0049	0.0038-0.0051
	3rd	0.633	0.584	-	0.0064-0.010
	4th	0.861	0.838	0.0046-0.0049	0.0041-0.0057
Torsion	1st	0.844	0.727	0.0018-0.0025	0.0021-0.0028
	2nd	-	1.440	-	0.0021-0.0030
	3rd	-	1.771	-	-
	4th	-	2.233	-	-

d) Meiko-nishi Bridge

Meiko-nishi Bridge is a three span continuous steel box girder bridge supported by two towers as shown in Fig. 5.115. The deck is supported by only cables so that the deck is free to move in the longitudinal direction. Prestressed cables are provided between the deck and the towers in order to control the natural period of the bridge and to prevent excessive relative displacement of the deck. A series of excitation tests was conducted at this bridge for flexural oscillations not only in the vertical direction but also in the transverse direction, and torsional oscillations by (1) a rotating eccentric-mass shaker, (2) impacts by heavy trucks running through the deck, and (3) pulling up and down a heavy mass. Fig. 5.116 compares the transverse flexural oscillations, which are important in seismic design, between the measured and the computed. The computed mode shapes agree well with the measured shapes.

Fig. 5.117 shows the dependence of damping ratios for the vertical modes, which were measured by impacts by heavy trucks, on the magnitudes of oscillation displacements. The damping ratios increase as the magnitude of displacements increases.

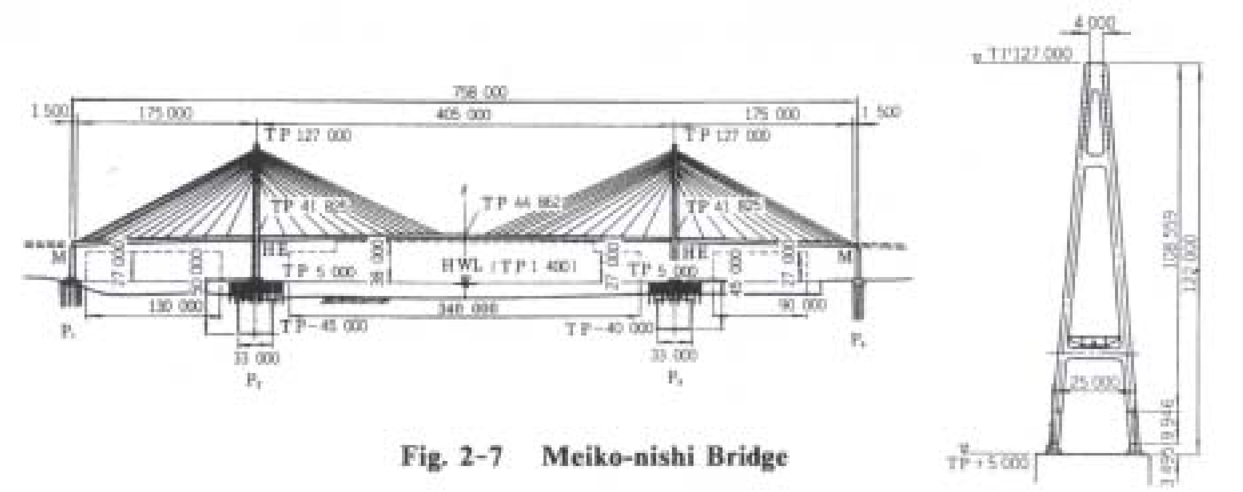

Fig. 5.115 Meiko-nishi Bridge

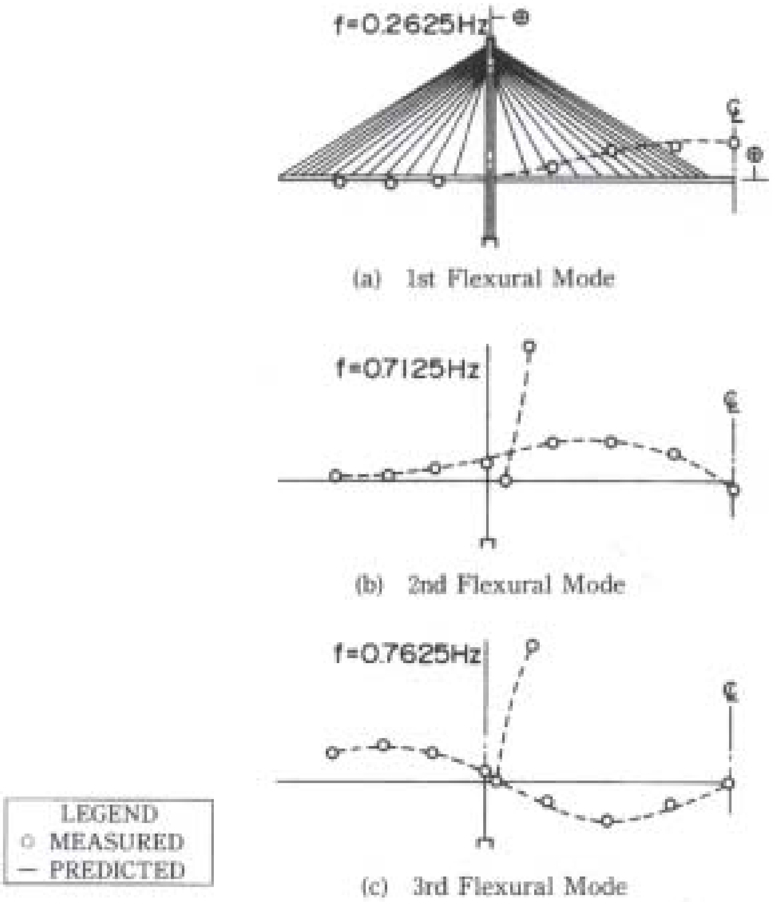

Fig. 5.116 Correlation of Computed Mode Shapes to the Measured for Flexural Oscillation in the Transverse Direction (Meiko-nishi Bridge)

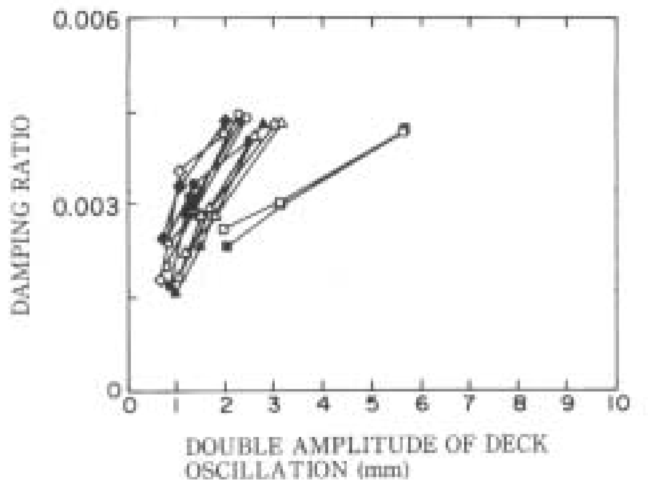

Fig. 5.117 Dependence of Damping Ratios on the Magnitude of Displacement of Oscillation

2) Natural Periods and Mode shapes of Cable Stayed bridges

In addition to the bridge described above, the similar tests have been conducted for many cable stayed bridges as shown in Table 5.6, in which the natural frequencies evaluated by the tests are presented. Plotting the lowest natural frequency vs. the center span length relations for the vertical and the transverse flexural oscillations, and torsional oscillations in Fig. 5.118 shows that there exist clear relations between the lowest natural frequencies and the center span lengths. A regression analysis provides the following relations (Kawashima, Unjoh and Tsunomoto 1991).

$$f_1{}^{BV} = 33.8L^{-0.763} \tag{5.63}$$

$$f_1{}^{BH} = 482L^{-1.262} \tag{5.64}$$

$$f_1{}^{T} = 17.5L^{-0.453} \tag{5.65}$$

where $f_1{}^{BV}$: lowest natural frequency for vertical flexural oscillation (Hz), $f_1{}^{BH}$: lowest natural frequency for transverse flexural oscillation (Hz), $f_1{}^{T}$: lowest natural frequency for torsional oscillation (Hz), and L : center span length (m). Because Eq. (5.64) is derived from only 4 data, this has to be reevaluated in the future by increasing the number of data. The rate of change of the natural frequencies depending on the center span length is highest in $f_1{}^{BH}$.

Table 5.6 Natural Frequencies Obtained by Field Forced Excitation Tests

Bridge		Onomichi	Toyosato	Arakawa	Kamome	Suehiro	Rokko	Suigo	Gassho	Yamato-gawa	Meiko-N	Matsugayma	Omoto-gawa	Bungo
Span		85+215+85	80+216+80	60+160+60	100+240+100	110+250+110	89+220+89	178+111	144+46+144	149+355+149	175+405+149	96	46+85+46	37+37
Cable		Radial	Fan	Harp	Multi	Fan	Fan	Harp	Fan	Harp	Fan	Fan	Harp	Harp
Deck		Steel Girder	Steel Box	Steel Girder	Steel Box	Steel Box	Steel Truss	Steel Box	Steel Box	Steel Box	Steel Box	PC Girder	PC Box	PC Hollow
Vertical Flexure	1st	0.58	0.52	0.75	0.47	0.47	0.94	0.45	0.64	0.34	0.33		1.99	1.60
	2nd	0.92	1.22	1.25		0.71	1.76	0.85	0.93	0.42	0.41		2.94	2.68
	3rd	1.38	1.92	1.91	0.99	1.07	2.42	1.26	1.31	0.63	0.73		5.3	3.30
	4th	1.62	2.48	2.41		1.26		2.03	1.41	0.86	0.81			5.30
	5th		3.33	2.83	1.46	1.62	2.68	2.56		1.03	0.95			5.69
	6th					2.09		3.38						
	7th						3.37	4.59		1.70				
	8th									1.86				
Torsion	1st	1.66	1.43	1.45		1.45	2.05	1.64	1.70	0.87	1.31	3.08		2.93
	2nd	2.94	3.25	2.80		2.89	3.92	2.98		1.67				3.68
	3rd		4.08	4.24		4.44	4.97	4.45						6.86
	4th							5.63						
Transverse Flexure	1st										0.26	1.51	1.52	5.50
	2nd										0.71		1.74	
	3rd										0.76		2.15	
	4th										1.01		2.35	

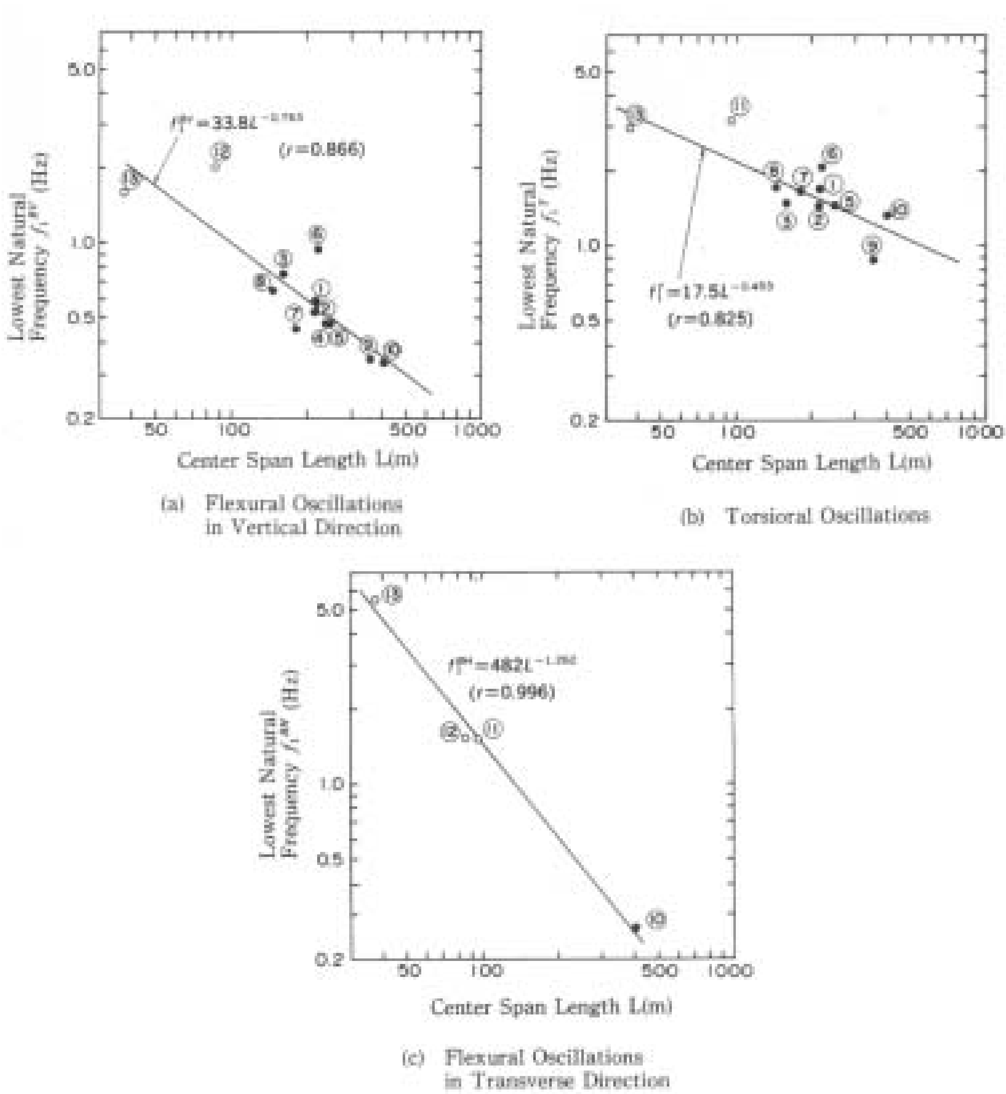

Fig. 5.118 Lowest Natural Frequencies vs. Center Span Length of Cable Stayed Bridges

3) Damping Ratios of Cable Stayed Bridges

Table 5.7 shows damping ratios of cable stayed bridges obtained from forced excitation tests. They were evaluated by either decays of free oscillations or resonance curves. Fig. 5.119 shows how the damping ratios depend on the mode numbers for flexural oscillations. Scattering of the relations depending on the number of modes and the directions is considerable. However the mode shape dependence of the damping rations is not considerable.

Table 5.7 Damping Rations Measured by Field Forced Excitation Tests

Bridge		Onomichi	Toyosato	Arakawa	Kamome	Suehiro	Rokko	Suigo	Gassho	Yamato-gawa	Meiko-N	Matsugayma	Omoto-gawa	Bungo
Vertical Flexure	1st	0.0080		0.0038	0.0121	0.0049		0.0110	0.0118	0.0037	0.0029		0.0140	0.0161
	2nd	0.0072		0.0054		0.0029	0.033	0.0059	0.0131	0.0049	0.0029		0.0126	0.0076
	3rd		0.0081	0.0081	0.0132	0.0029	0.011	0.0064	0.0154		0.0024			0.0423
	4th		0.0138			0.0024	0.015	0.0102	0.0169	0.0048	0.0024			0.0068
	5th				0.0089	0.0019		0.0124						0.0102
	6th							0.0100						
	7th						0.013	0.0132						
		0.0076	0.0110	0.0057	0.0115	0.0030	0.018	0.0099	0.0143	0.0045	0.0027		0.0134	0.0166
Torsion	1st	0.0056	0.0113			0.0025	0.0106	0.0092	0.0060	0.0019	0.0032			0.0121
	2nd	0.0048	0.0132			0.0089		0.0091						0.0628
	3rd						0.0134	0.0169						0.0126
	4th							0.0096						
		0.0053	0.0123			0.0057	0.0121	0.0111	0.0060	0.0019	0.0032			0.0138
Transverse Flexure	1st										0.0092	0.035	0.020	0.0317
	2nd										0.0025			
	3rd										0.0016		0.111	
	4th										0.0008			
											0.0035		0.0236	0.0317
Averaged		0.0064	0.012	0.0057	0.011	0.0038	0.016	0.010	0.013	0.0038	0.0030	0.035	0.018	0.017

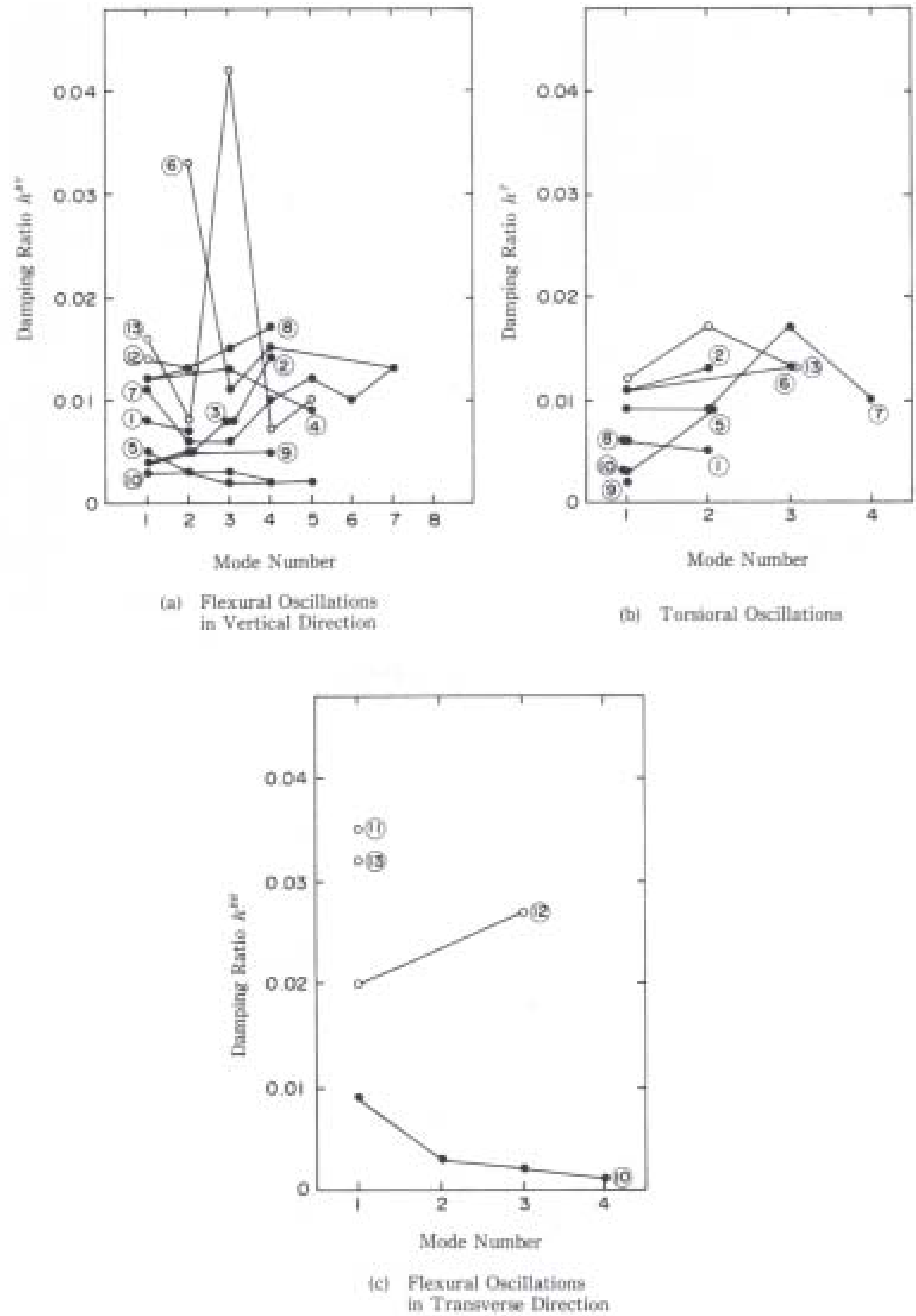

Fig. 5.119 Variation of Damping Ratios depending on Mode Numbers

To study the dependence of damping ratios on the center span lengths, the damping ratios which are averaged over all modes measured are plotted against the center span length L in Fig. 5.120. The damping ratios decrease as the center span lengths increase as (Kawashima, Unjoh and Azuta 1988, Kawashima, Unjoh Tsunomoto 1991)

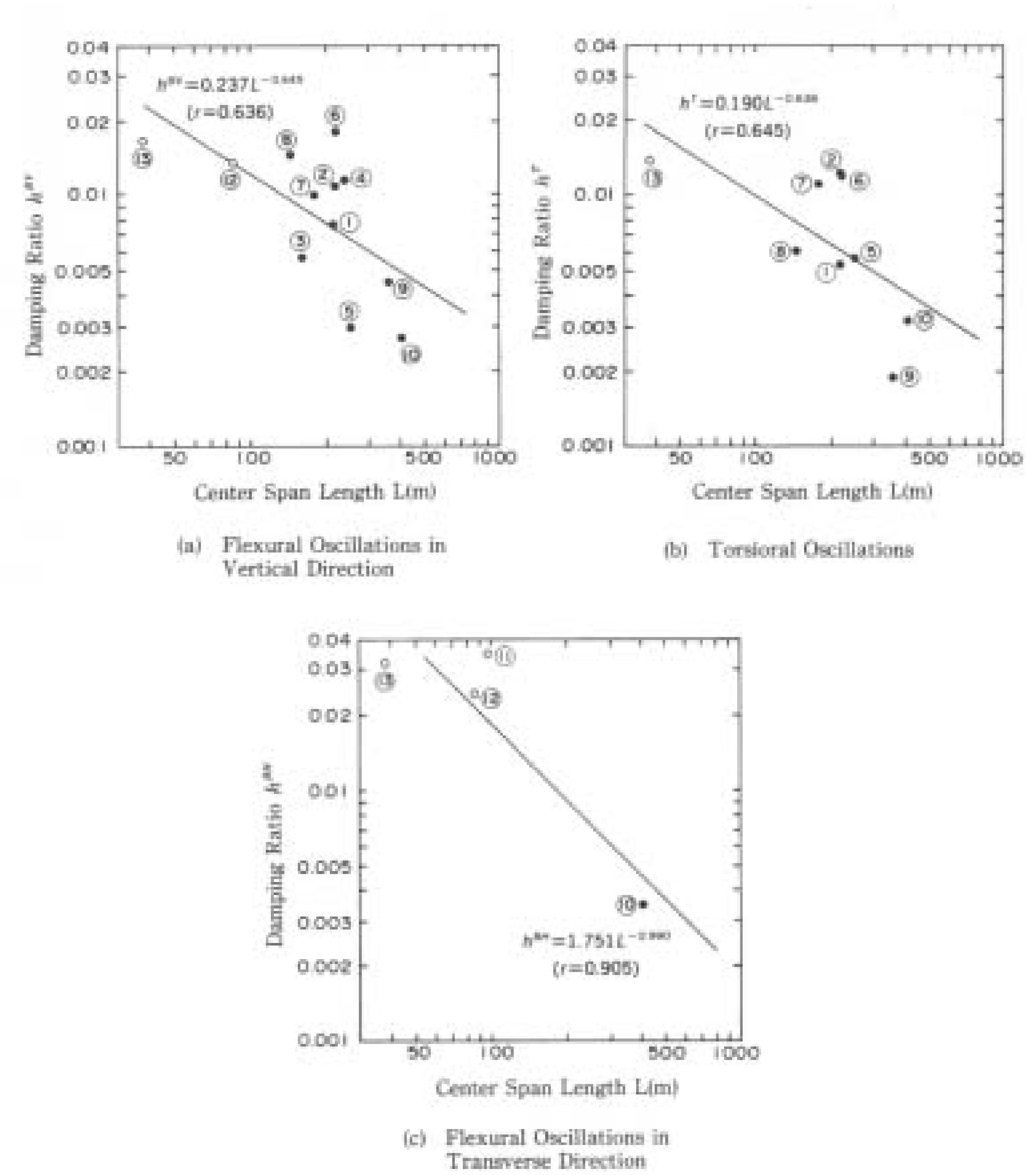

Fig. 5.120 Damping Ratios vs. Center Span Lengths of Cable stayed Bridges

$$\xi^{BV} = 0.237L^{-0.645} \tag{5.66}$$

$$\xi^{BH} = 1.751L^{-0.990} \tag{5.67}$$

$$\xi^{T} = 0.190L^{-0.638} \tag{5.68}$$

where ξ^{BV}: damping ratio for vertical flexural oscillations, ξ^{BH}: damping ratio for transverse flexural oscillations, and ξ^{T}: damping ratio for torsional oscillations. Because Eq. (5.67) was derived from only 4 data, its validity has to be reevaluated by increasing the number of data. The dependence of the damping ratios on the center span lengths is the highest in ξ^{BH} with the dependence in ξ^{BV} and ξ^{BH} being nearly the same.

Because there exist clear relations between the natural frequencies and the center span lengths, and between the damping ratios and the center span lengths, there must exist relations between the damping ratios and the natural frequencies. Fig. 5.121 shows the relations between the damping ratios (ξ^{BV}, ξ^{BH}, and ξ^{T}) and the natural frequencies (f_1^{BV}, f_1^{BH}, and f_1^{T}). Regression analysis provides the following relations,

$$\xi^{BV} = 0.0053 + 0.0060\, f_1^{BV} \tag{5.69}$$

$$\xi^{BH} = 0.0153 + 0.0037\, f_1^{BH} \tag{5.70}$$

$$\xi^{T} = -0.0016 + 0.0057\, f_1^{T} \tag{5.71}$$

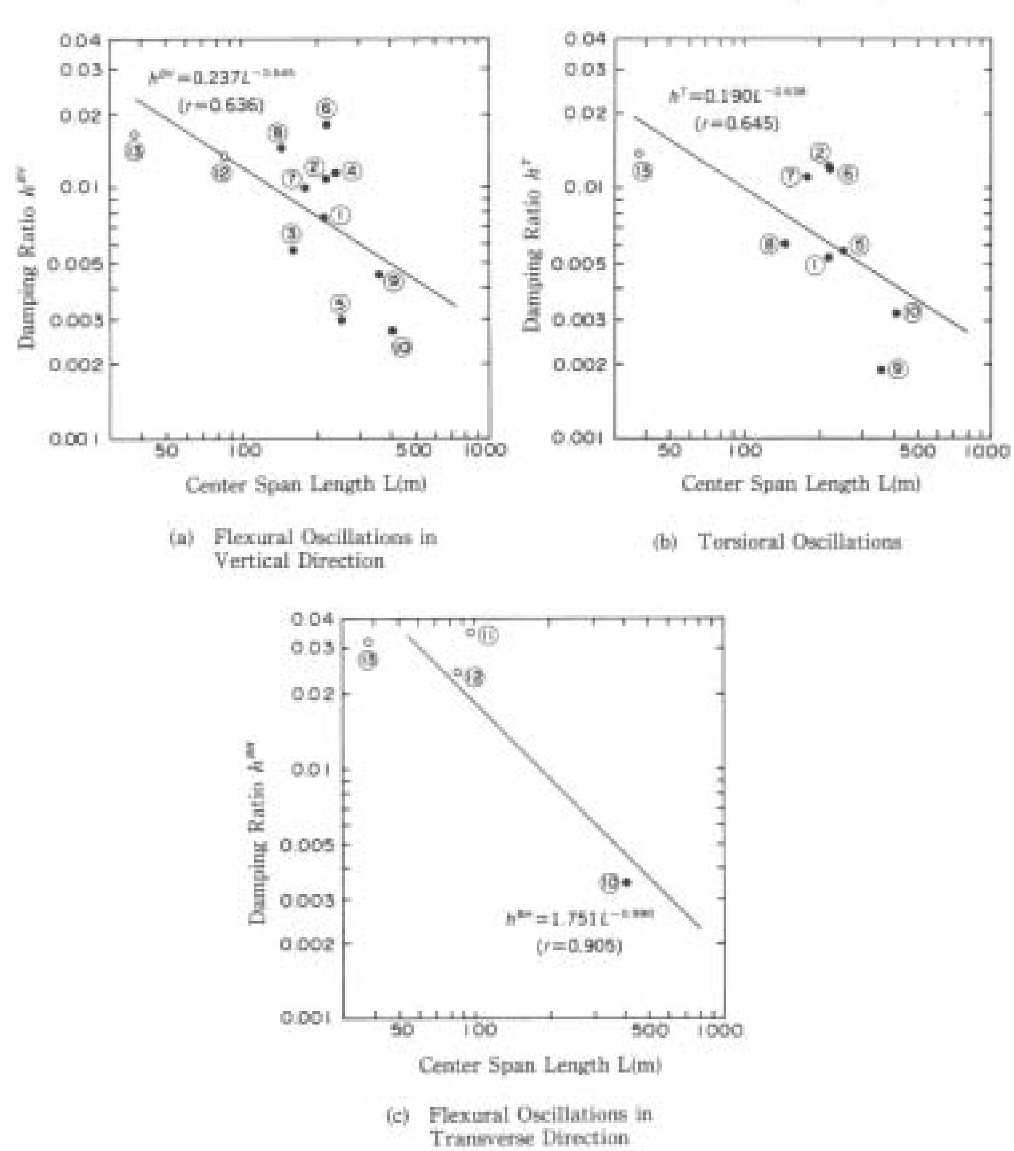

Fig. 5.121 Damping Ratio vs. Natural Frequencies of Cable stayed Bridges

4) Analysis of Damping Ratios of a Cable Stayed Bridge based on Measured Records
a) Dynamic Characteristics of Suigo Bridge

Suigo Bridge is a 290 m long two-span continuous steel cable stayed as shown in Fig. 5.122. The deck consists of a steel box girder and it is rigidly connected to a 47.2 m tall single steel tower. The superstructure is supported by fixed bearings at the intermediate support (A3, refer to Fig. 5.122) and movable bearings at the both ends. Two caisson foundations and a pile foundation support the superstructure.

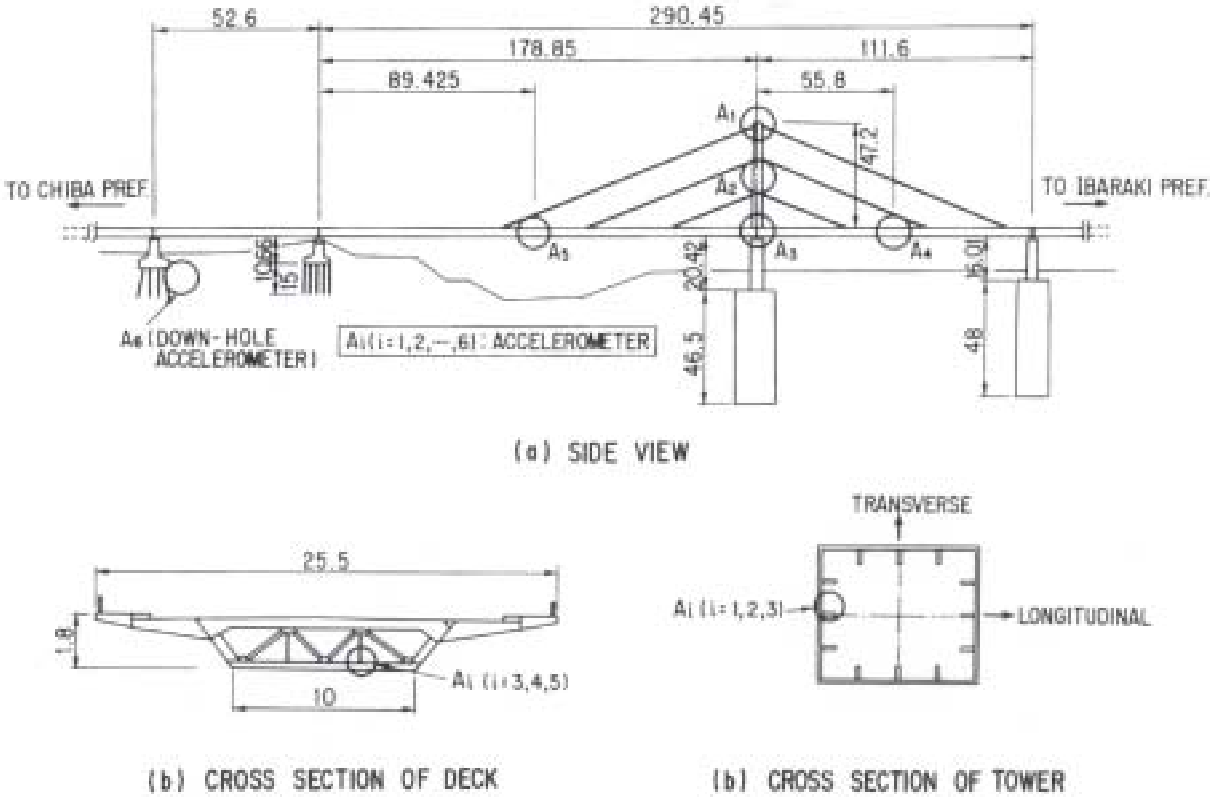

Fig. 5.122 Suigo Bridge

A series of forced excitation tests was conducted at this bridge to study the aero dynamic stability. Two electric exciters, which produce sinusoidal forces in the vertical direction by rotating a set of unbalanced masses, were set on the deck, and the bridge was excited for vertical flexure or torsional oscillations by synchronizing and anti-synchronizing the two exciters. Natural mode shapes and natural frequencies were estimated for lower significant modes from steady-state oscillation of the superstructure.

Fig. 5.123 shows an example of resonant curves of response acceleration excited in the vertical direction. Mode shape are obtained by plotting the measured response accelerations at various locations along the members as shown in Fig. 5.124, in which computed mode shapes using a linear analytical model described later are presented. The computed mode shapes agree well with the measured mode shapes.

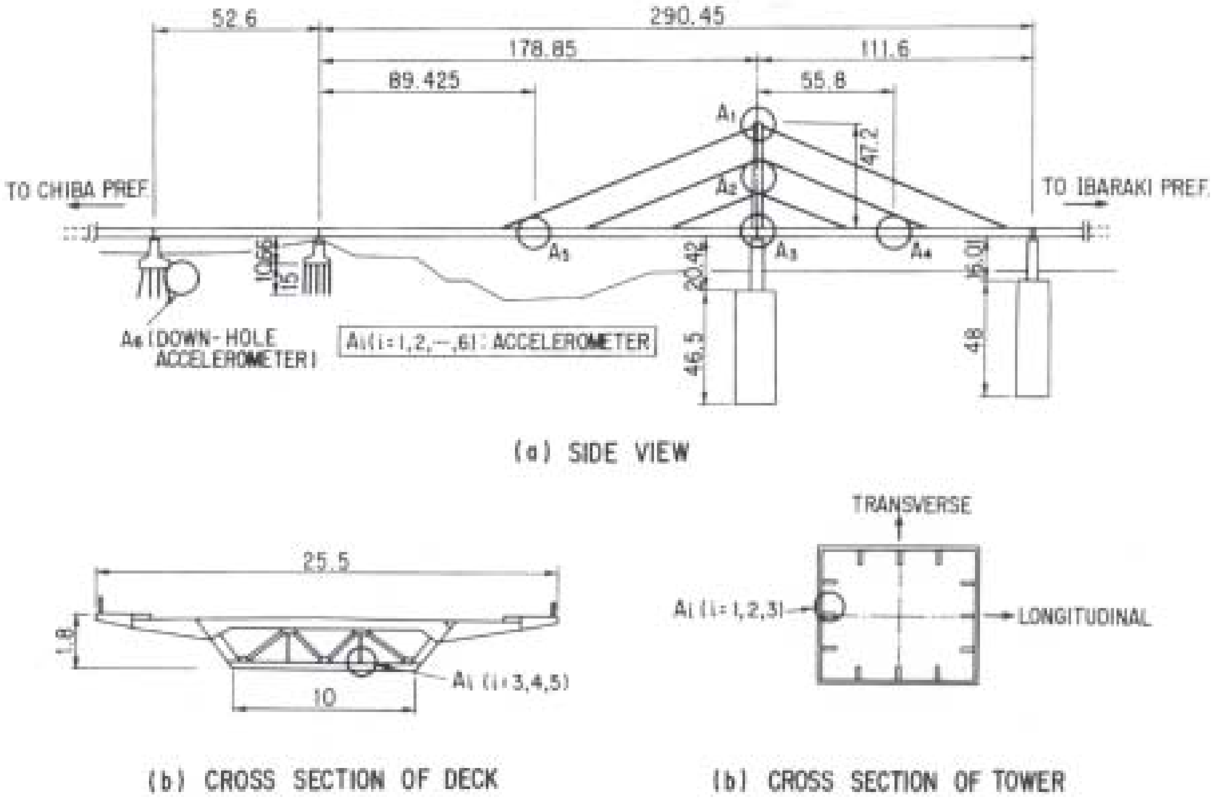

Fig. 5.122 Suigo Bridge

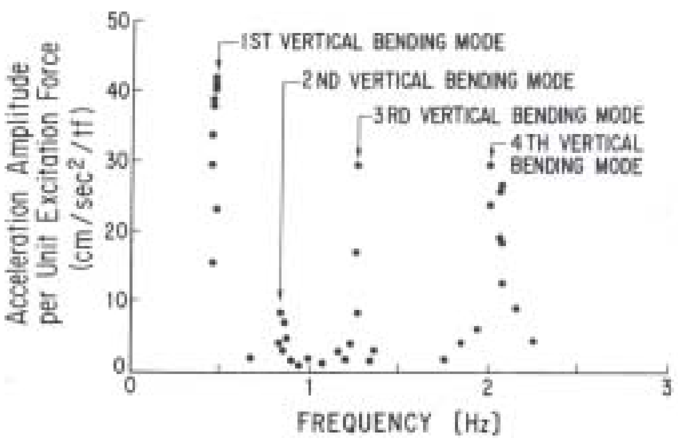

Fig. 5.123 Resonant Curve by Forced Excitation Test (Suigo Bridge)

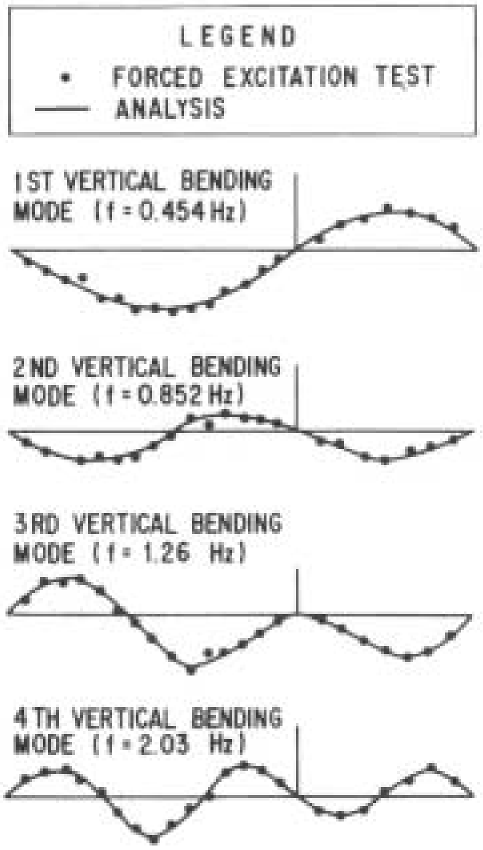

Fig. 5.124 Comparison of Natural Mode Shapes between Measured and Computed (Suigo Bridge)

Damping ratios are estimated from logarithmic decays of the free oscillations from steady-state vibrations. Damping ratios, which are estimated from the logarithmic damping ratio, depend on the mode shapes as shown in Table 5.8.

Table 5.8 Damping Ratios Estimated from Free Oscillation Tests (Suigo Bridge)

Mode	1st	2nd	3rd	4th	5th	6th	7th	Averaged
Vertical Flexure	0.011	0.0059	0.0064	0.0102	0.0124	0.0100	0.0132	0.0099
Torsion	0.0092	0.0091	0.0168	0.0096	-	-	-	0.0112

b) Measured Records during Past Earthquakes

Recording of bridge response has been conducted at this bridge since 1986. Two horizontal components force-balanced accelerometers are installed as shown in Fig. 5.43 at (1) top of the tower (Al), (2) the mid-height of the tower (A2), (3) bottom of the tower (A3), (4) and (5) centers of both girders (A4 and A5), and (6) 15 m below the ground surface 230 m apart from the tower (A6).

Large response accelerations were recorded by (1) M=6.5 event in 1986 (EQ-6), (2) M=6.7 event in 1987 (EQ-16), and (3) M=6.7 event in 1987 (EQ-33). Peak response accelerations during these three events are shown in Table 5.9. Sufficiently large accelerations as shown in Fig. 5.125 were recorded by an M=6.7 event (EQ-33) which occurred at 62 km from the bridge in 1987. Of particular importance is the large response acceleration at the top of the tower (A1) in the transverse direction. Peak acceleration at A1 reached to 1,000 gal. Because the peak acceleration at the mid-height (A2) and the bottom (A3) of the tower is 471 gal and

173 gal, respectively, it is obvious that the tower oscillated with a cantilevered mode shape. In the longitudinal direction, the peak acceleration is 446 gal at the top of the tower (A1), 297 gal at the mid-height (A2) and 216gal at the bottom of the tower (A3), respectively. The response accelerations in the longitudinal direction are approximately 50 % smaller than the response accelerations in the transverse direction.

Table 5.9 Peak Accelerations Recorded during Three Events

Earthquake	A1		A2		A3		A4		A5		A6	
	LG	TR	LG	TR	LG	TR	LG	TR	LG	TR	LG	TR
EQ-6	189	217	75	111	55	34	61	-	62	77	13	13
EQ-16	238	322	109	218	87	54	91	-	100	104	23	22
EQ-33	446	1,000	297	471	216	173	257	-	247	363	99	114

1) LG and TR represent the longitudinal and the transverse directions, respectively
2) Records in the transverse direction at A4 were not obtained due to malfunction

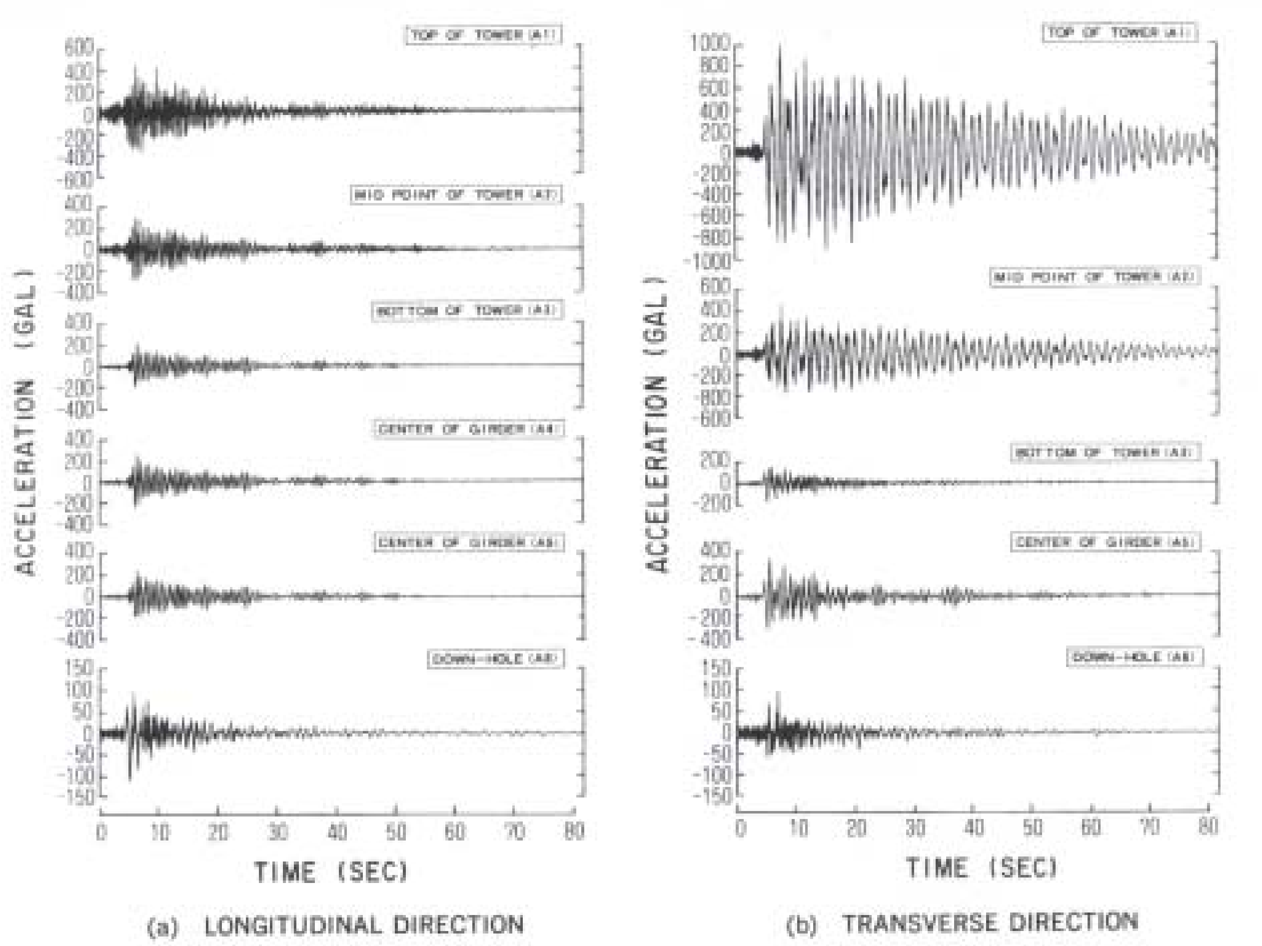

Fig. 5.125 Acceleration Records during an M6.7 Event at Suigo ridge

c) Dynamic Characteristics based on the Measured Accelerations

Fig. 5.126 shows the Fourier spectra of the acceleration records presented in Fig. 5.125 (EQ-33). Predominant frequencies in the response of the deck and the tower are 1.51 Hz in the longitudinal direction and 0.72 Hz, 0.87 Hz and 1.22 Hz in the transverse direction. Predominant frequency in the ground accelerations is 0.87 Hz in both the longitudinal and the transverse directions. One can note that 4.60 Hz in the longitudinal direction and 5.26 Hz in the transverse direction are also predominant in the response of the top of the tower (A1).

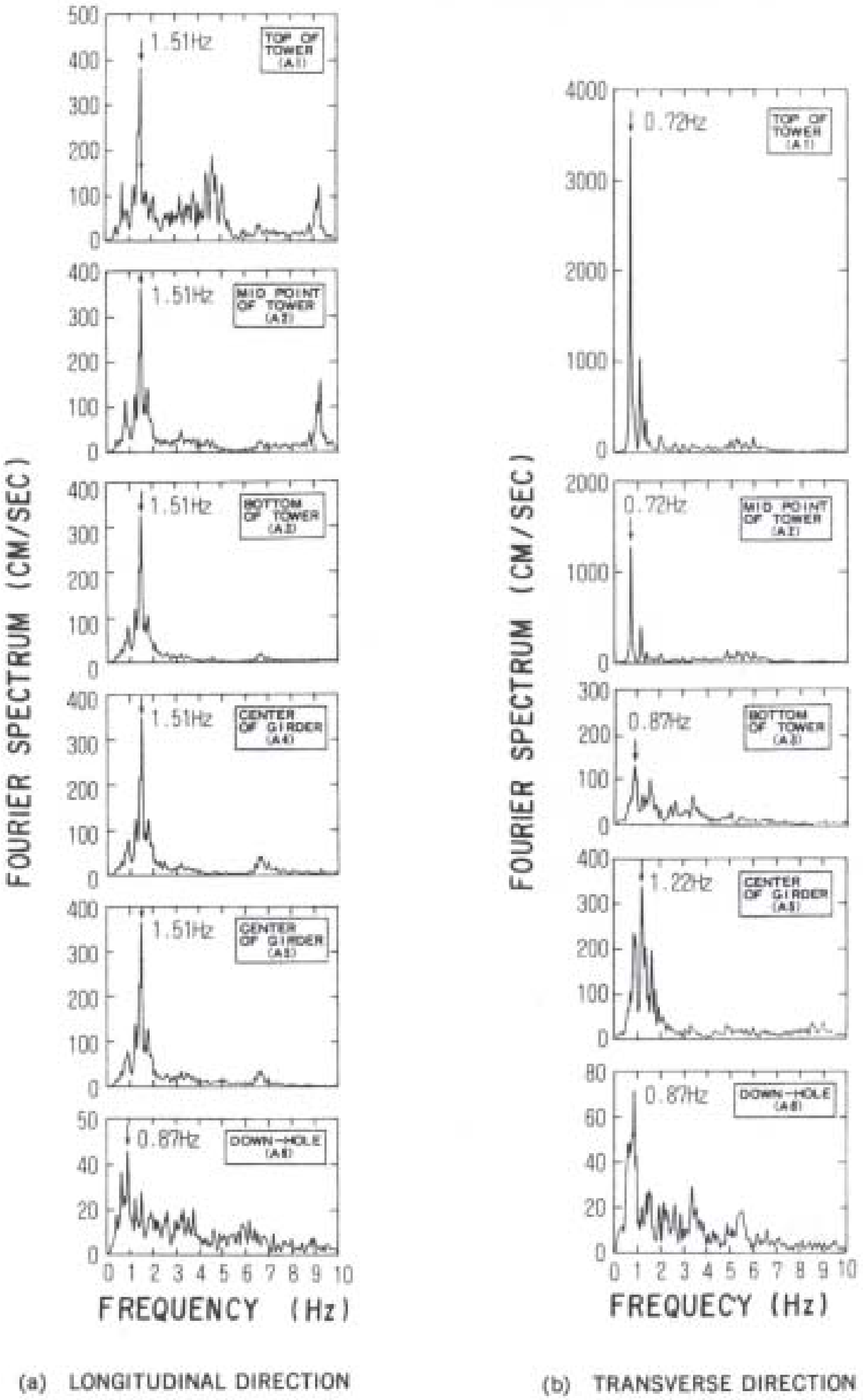

Fig. 5.126 Fourier Spectra of Measured Response Acceleration at Suigo Bridge

To evaluate the vibration mode of the bridge, the intensities of accelerations at the same instance after processed by a band-path filter are plotted as shown in Fig. 5.127. The first translational mode with a predominant frequency of 1.51 Hz and the first flexural mode of the tower with a predominant frequency of 4.60 Hz are observed in the longitudinal direction, while the first and the second flexural modes of the tower with predominant frequencies of 0.72 Hz, 1.22 Hz, and 5. 26 Hz are observed in the transverse direction.

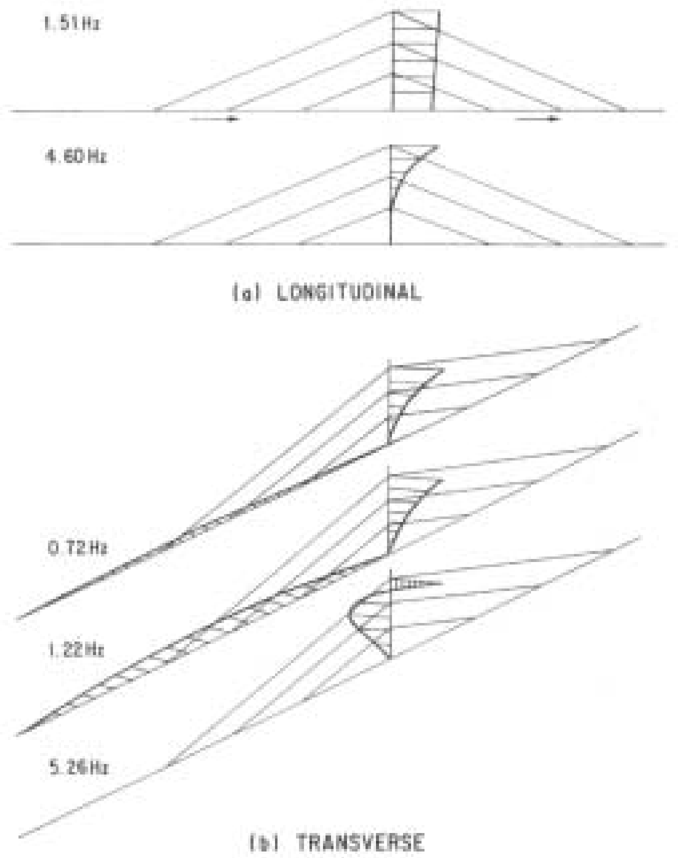

Fig. 5.127 Vibration Modes Evaluated from Measured Response Accelerations

To analyze the natural frequencies and the mode shapes, Suigo Bridge is idealized by a linear analytical model as shown in Fig. 5.1128. The cables are idealized as elastic beams with zero stiffness for flexure. Both ends of the deck, which are supported by the movable bearings, are assumed free to move in the longitudinal direction and fixed in the transverse direction. Friction resulted from movements of the deck relative to the substructures at the movable bearings is disregarded. Fig. 5.129 shows computed mode shapes and natural frequencies. The 1st, 2nd, 3rd, and 4th vertical flexural modes which were identified for the forced excitation test in Fig. 5.124 correspond to 1st, 6th, 9th, and 10th predicted modes, respectively, in Fig. 5.129. On the other hand, the 1st, 2nd, and 10th modes in the transverse direction in Fig. 5.129 correspond to the modes in Fig. 5.127 with predominant frequencies of 0.72Hz, 1.22 Hz, and 5.26 Hz, respectively. However in the computed modes in Fig. 5.129, there is not the translational mode in the longitudinal direction (predominant frequency = 1.51 Hz) which is identified from the measured accelerations (refer to Fig. 5.127). This is because only the superstructure is idealized in the analysis in Fig. 5.128. By including substructures into the analytical model, a rocking mode of the foundation with a natural frequency of 1.52 Hz is obtained, and this corresponds to the translational mode with the predominant frequency of 1.51 Hz in Fig. 5.127.

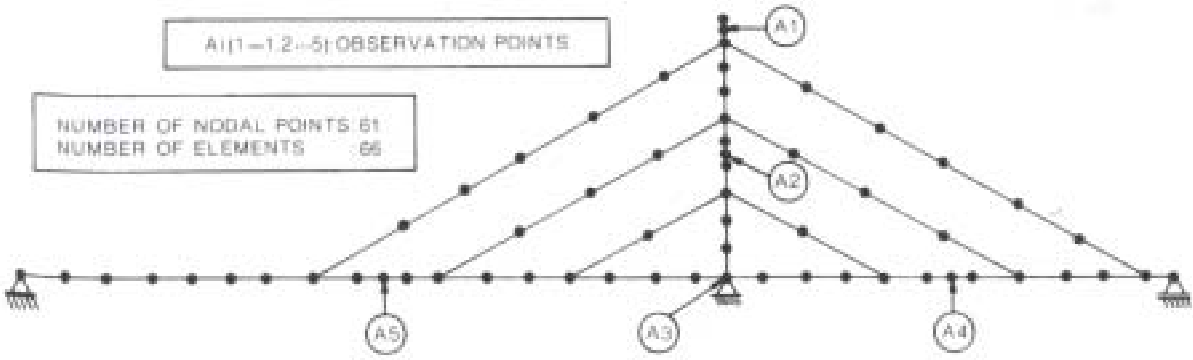

Fig. 5.128 Analytical Model of Suigo Bridge

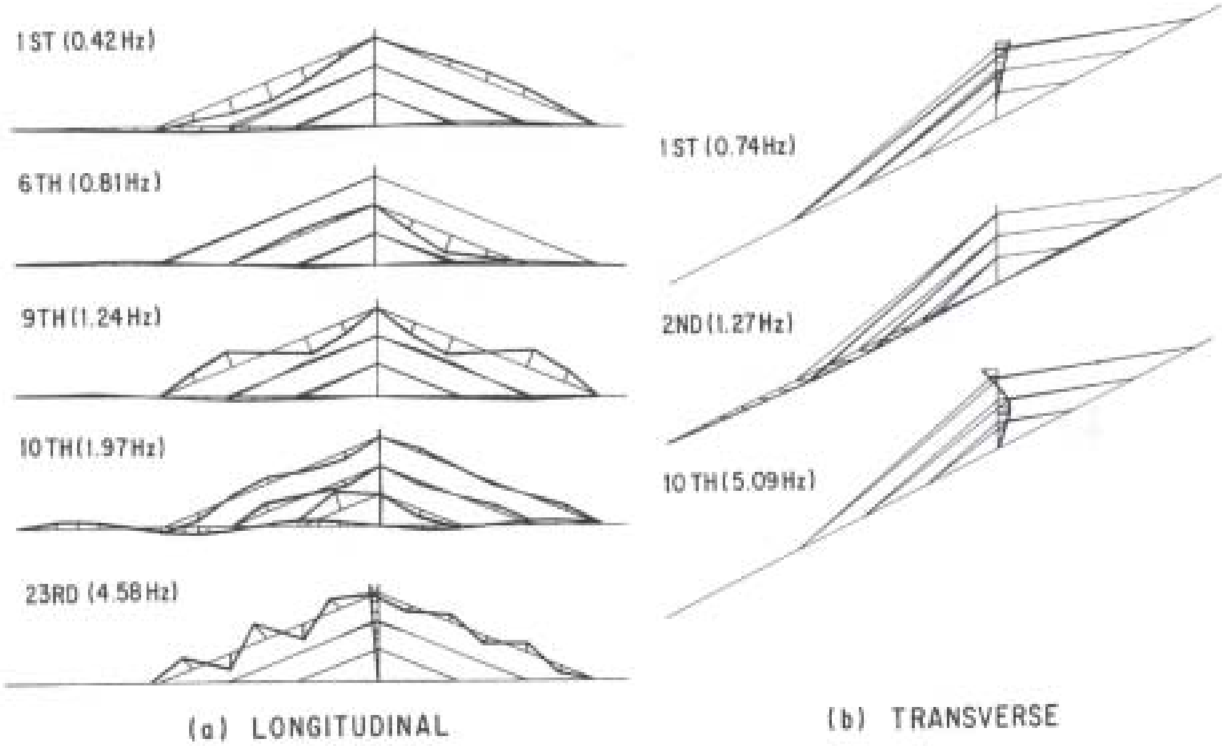

Fig. 5.129 Computed Mode Shapes and Natural Frequencies

d) Dynamic Response Analysis of Suigo Bridge

Measured seismic responses of Suigo Bridge are correlated with analysis by varying damping ratios assumed in the analysis (Kawashima, Unjoh and Azuta 1990). Because the response acceleration at the bottom of the tower (A3 point) was recorded, it is prescribed at A3 to compute responses in the longitudinal direction assuming that no input motions are applied at both ends supported by the movable bearings. On the other hand, the measured record at A3 is prescribed at A3 and both ends of the deck to compute responses in the transverse direction assuming that the same input motions apply at the three supports. It is noted that the analytical model in Fig. 5.128 does not include the substructures. As described above, including the substructures in the analytical model yields the rocking mode of substructures which results in the translational mode of the tower. However, because the response measured at A3 which includes this translational mode of the tower as a result of the rocking response of the substructures is applied as an input motion, disregard of this mode does not cause an error in the computation of the response of the superstructure.

Damping ratios in the analysis are varied as 0.0, 0.01, 0.02, and 0.05. Analysis is conducted for the three records in Table 5.9. As an example, Fig. 5.130 shows a comparative plot of the response accelerations between the measured and the computed at the top of the tower (A1) and the center of the deck (A5) for EQ-33. A damping ratio of 0.05 yields a close correlation to the measured responses of the tower (A1) and the deck (A5) in the longitudinal direction. The damping ratio of 0.05 also yields a good correlation for the deck response (A5) in the transverse direction. However, for the response of the tower (A1) in the transverse direction, the 0.05 damping ratio yields a considerable underestimation, and a damping ratio of 0.0 yields a better agreement. Table 5.10 shows the damping ratios which yield the best correlation for the measured accelerations. They are 0.02 and 0-0.01 for the responses of the tower in the longitudinal and the transverse directions, respectively, and are 0.05 for the responses of the deck in both the longitudinal and the transverse directions.

Table 5.10 Damping Ratios which yield the Best Correlation for Measured Responses

Records	Longitudinal				Transverse		
	A1	A2	A4	A5	A1	A2	A5
EQ-6	0.02	0.05	0.05	0.05	0-0.01	0.01	0.05
EQ-16	0.02	0.05	0.05	0.05	0-0.01	0.01	0.05
EQ-33	0.05	0.05	0.05	0.05	0-0.01	0.01	0.05

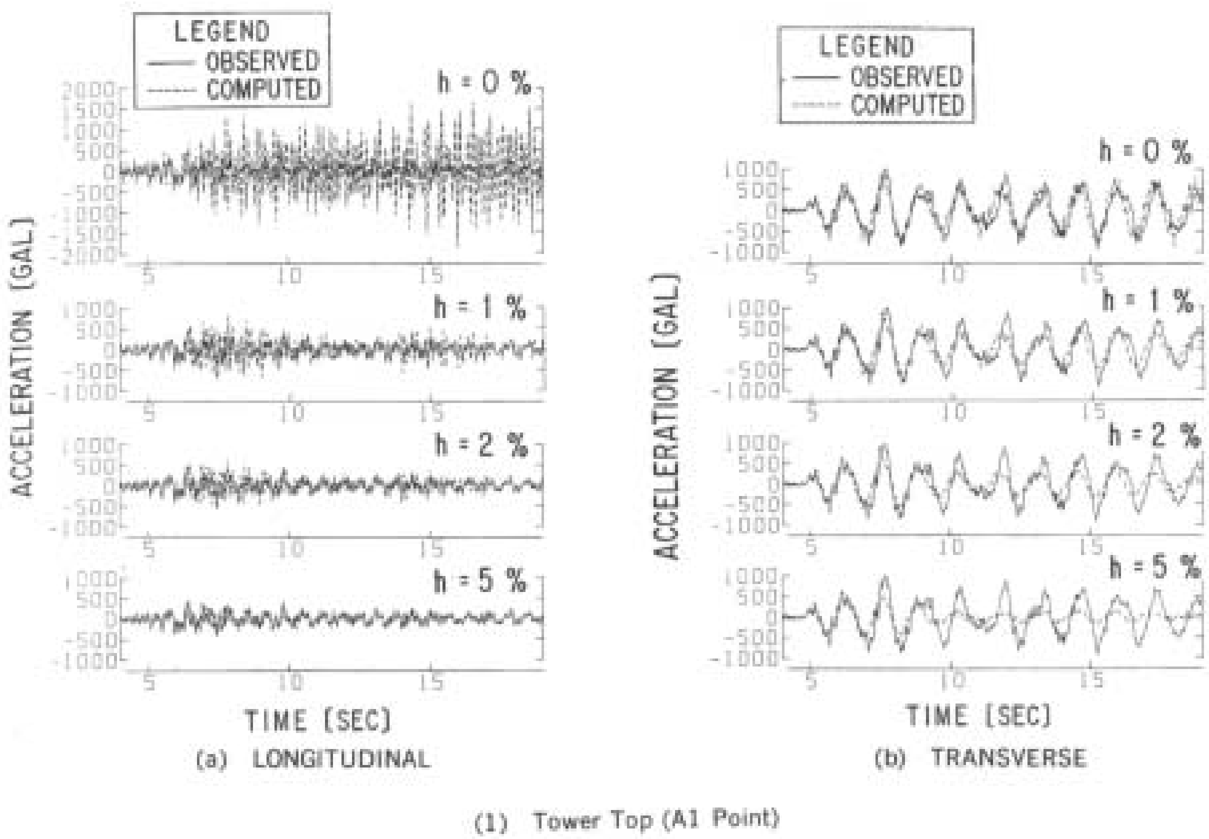

Fig. 5.130 Comparison of Response Accelerations between Measured and Computed (1)

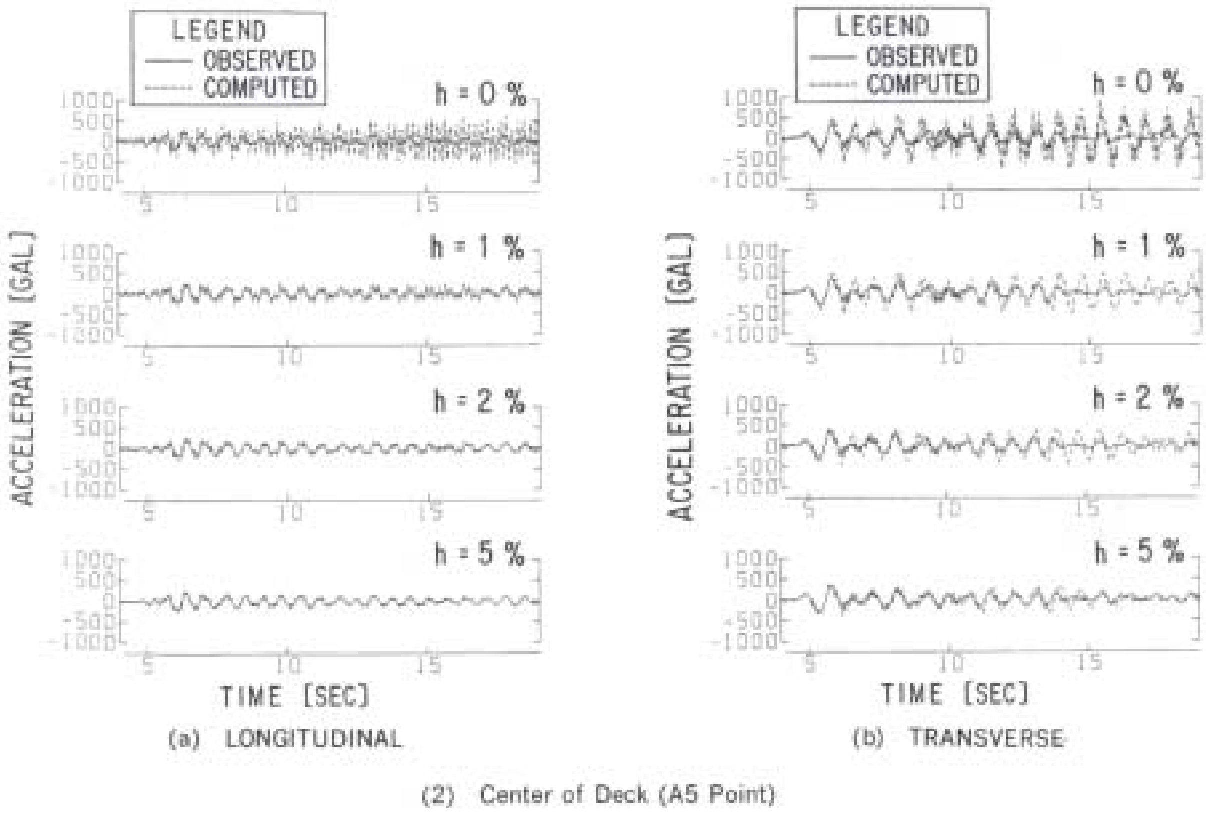

Fig. 5.130 Comparison of Response Accelerations between Measured and Computed (2)

It is important that the damping ratios which provide the best correlation depend on the structural components and the directions. This results from the effect of cables on the response of the tower. Since the flexural rigidity of the cables is negligibly small, the tower is nearly free to oscillate as a free-standing column in the transverse direction. It is reasonable to have a very small damping ratio in such an oscillation as a free-standing column. On the other hand, the tower response is coupled with the deck response by the cables in the longitudinal direction, which results in a larger damping ratio of 0.05.

Consequently, responses were computed using damping ratios estimated by Eq. (2.6), in which 0.02 and 0.0 are assumed for the tower in the longitudinal and transverse directions, respectively, and 0.05 is assumed for the deck in both the longitudinal and the transverse directions. Fig. 5.131 shows the correlation of response accelerations thus computed. The computed responses agree well with the measured responses at both the tower and the deck. This shows the importance of providing appropriate damping ratios depending on the structural components and the directions.

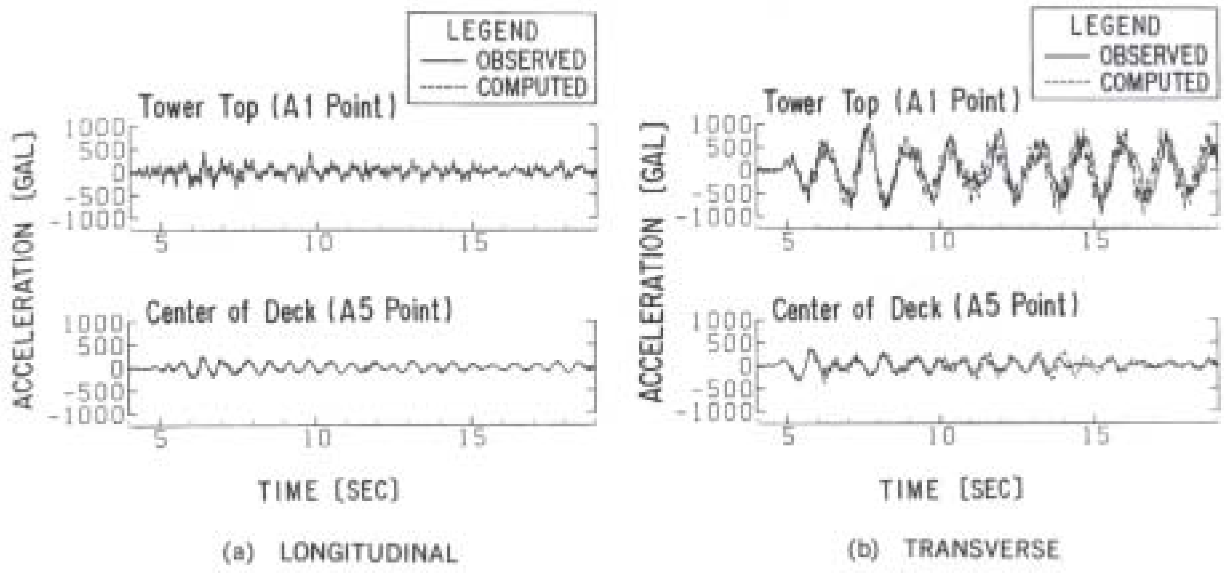

Fig. 5.131 Computed Responses using Damping Ratios Estimated by Eq. (2.6)

5) Damping Ratios Resulting from Energy Dissipation at Movable Bearings

Damping of cable stayed bridges results from various sources of energy dissipation such as viscous damping, hysteretic damping of materials, structural damping, radiational damping at foundations, and energy dissipation at movable supports. Among those factors, energy dissipation at movable bearings contributes to change damping ratio depending on the magnitude of oscillation displacement in the longitudinal direction during forced excitation tests. Since upper and lower shoes are locked during longitudinal oscillations with very small amplitudes, sliding between the upper and the lower shoes does not occur at movable bearings. As the oscillation amplitude increases, sliding occurs resulting in energy dissipation due to friction forces between upper and lower bearings at movable bearings. Since this yields a unique damping characteristics, the effect of energy dissipation at movable bearings is described here.

A friction force at movable supports is idealized by Coulomb friction force. Friction force is a self-equilibrium force which acts on a contact plane of bearing in proportion to the contact force. As shown in Fig. 5.132, direction of the friction force developed when the relative movement at the contact plane Δu occurs is opposite to the direction of the relative velocity developed at the contact plane $\Delta\dot{u}$, i. e., the friction force $F_r{}^I$ and $F_r{}^J$ at points *I* and *J*, respectively, are expressed as

$$F_r{}^I = -F_r{}^J = \mu \cdot N \cdot sign(\Delta\dot{u}) \quad \text{when} \quad \Delta\dot{u} \neq 0$$
$$-\mu N < F_r{}^I = -F_r{}^J < \mu N \quad \text{when} \quad \Delta\dot{u} = 0 \tag{5.72}$$

where

$$\Delta u = u_J - u_I \tag{5.73}$$

in which μ : coefficient of Coulomb friction, N : contact force, and u_I and u_J : displacement at points *I* and *J*, respectively.

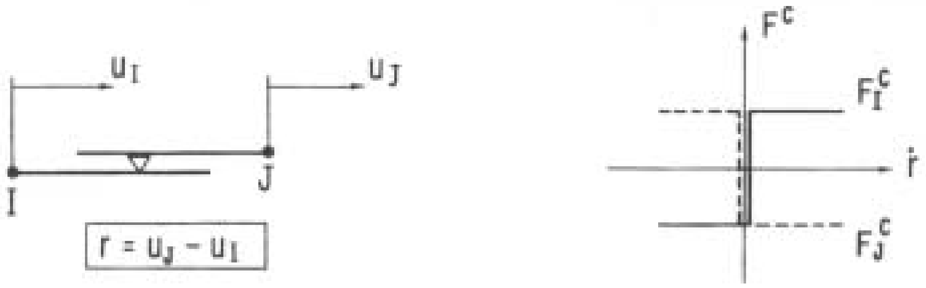

Fig. 5.132 Coulomb Friction Force

To evaluate the effect of friction forces at movable supports in the longitudinal oscillation, a cable stayed bridge is modeled by a discrete analytical model including the friction forces by Eq. (5.72). No damping forces other than the friction forces at movable supports are included in the analysis to isolate the effect of friction force. The equations of motion including the friction force is formulated in an incremental form, and can be solved for each time increment according to the standard dynamic analysis procedure (refer to Chapter 2). Iteration to approve equilibrium of the equations of motion is conducted when it is necessary.

Two cable stayed bridges as shown in Fig. 5.133 are analyzed (Kawashima and Unjoh 1989). One is a 380 m long two span continuous cable stayed bridge (A1-bridge) supported by a single tower. Fourteen cables are placed symmetrically in “fan” form. The girder is rigidly connected to the tower, with two ends being supported by movable bearings. The mass of the girder, the tower and the cables is 4435t, 734t and 120t, respectively. Reaction force at the two end supports due to the dead weight of the superstructure is 563 tf which is regarded as the contact force N defined by Eq. (5.72). The other is a 755 m long three span continuous cable stayed bridge (B-bridge) with a symmetrical distribution of mass and stiffness. The girder is not connected to the towers, but prestressed cables are set between the deck and the two towers for controlling the natural period of the bridge and for preventing excessive relative displacements to take place between the deck and the towers. The mass of the girder, the towers and the cables are 9630t, 1734t and 604t, respectively. The reaction forces at the two end supports due to the dead weight of the superstructure is 203tf. Soil-foundation interaction is disregarded in both bridges for simplicity.

Fig. 5.134 shows predominant mode shapes of the two bridges. Fifth (natural period T =0.52 s) and 3rd modes (T=2.11 s) are predominant in the A-Bridge and the B-Bridge, respectively.

Fig. 5.135 shows numerically computed decays of the free oscillations and damping ratios determined from the decays by Eq. (5.61) for 5th mode of the A-Bridge and 3rd mode of the B-Bridge. The free oscillations are generated by releasing the bridges with zero velocity from a laterally displaced positions with 300 mm lateral displacements at the deck. The coefficient of friction μ equals 0.1 and 0.2. The oscillation amplitudes decrease nearly linearly with time in both bridges. The damping ratios determined by logarithmic damping ratios using Eq. (5.61) have some fluctuations, but they increase as the oscillation amplitudes decrease. Fig. 5.136 shows how the damping ratios depend on the amplitudes of deck displacement. The damping ratio at an oscillation amplitude depends on bridges and mode shapes. When the coefficient of friction is 0.1, the damping ratio at 100 mm deck displacement is 0.005 in the A-Bridge and 0.025 in the B-Bridge. Since damping ratios of cable stayed bridges are very small, this level of damping ratios is important in the evaluation of seismic response of cable stayed bridges.

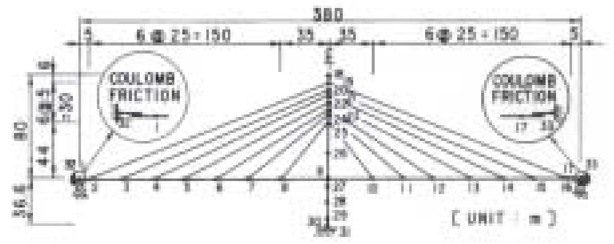

(a) Two Span Continuous Cable-Stayed Bridge (A1 and A2-Bridge)

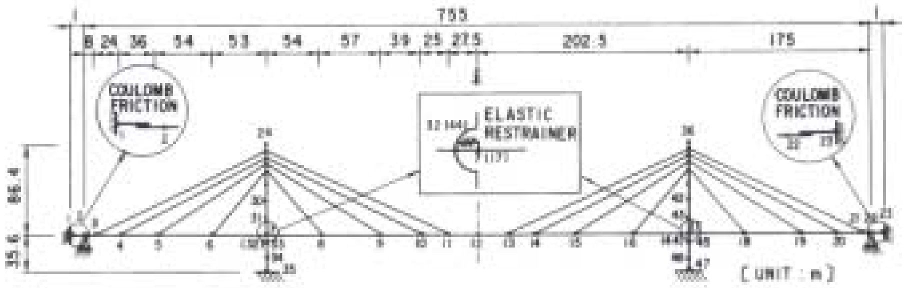

(b) Three Span Continuous Cable-Stayed Bridge (B-Bridge)

Fig. 5.133 Models of Two Cable Stayed Bridges

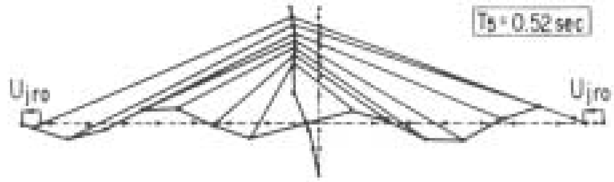

(a) 5th Mode of A-Bridge

(b) 3rd mode of B-Bridge

Fig. 5.134 Predominant Mode Shapes in the Longitudinal Direction

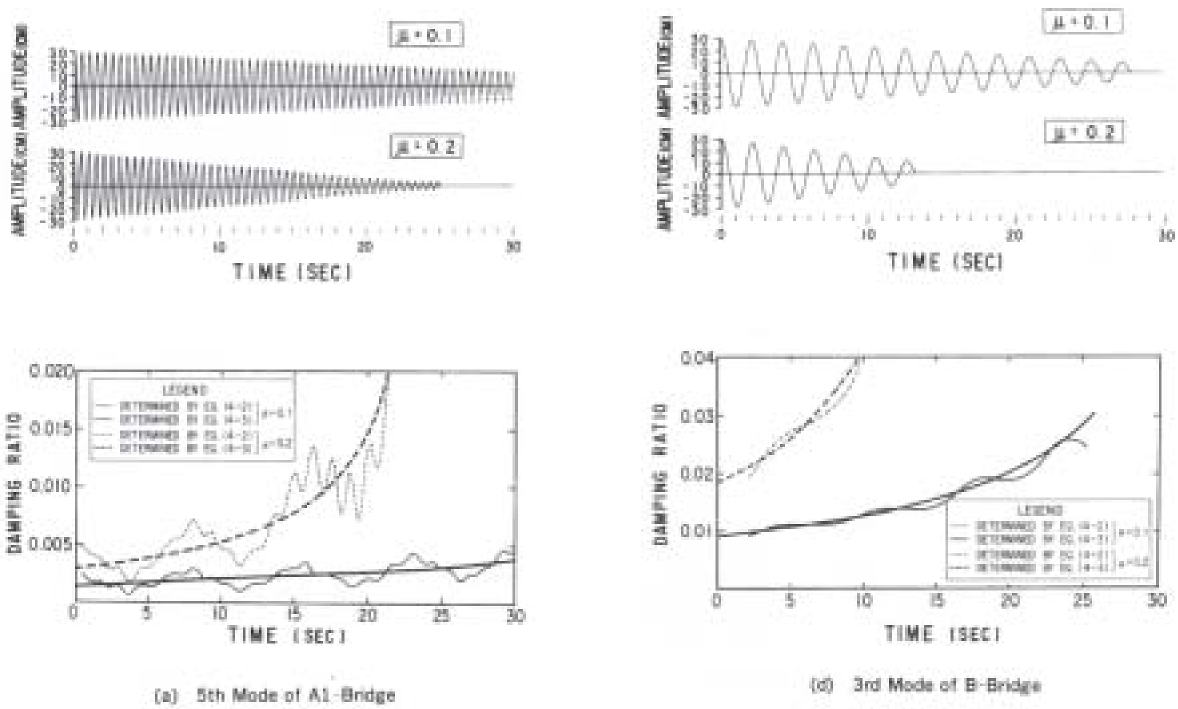

(a) 5th Mode of A-Bridge (b) 3rd Mode of B-Bridge

Fig. 5.135 Decays of Free Oscillation and Damping Ratio Computed from the Decay

Energy dissipation $\Delta E_j{}^m$ resulted from a friction force during one cycle of the j-th mode between a time interval from t_m and $t_m + T_j$ may be obtained as

$$\Delta E_j{}^m = \int_{t_m}^{t_m+T_j} |F_r| d\Delta u \tag{5.74}$$

where T_j : natural period of j-th mode, F_r : the friction force given by Eq. (5.72), and Δu : relative displacement between a deck and a substructure at a movable bearing defined by Eq. (5.73). Since bearings are supported by rigid substructures in this analysis (refer to Fig. 5.133), $\Delta E_j{}^m$ by Eq. (5.74) can be written as

$$\Delta E_j{}^m = 4 \sum_r F_r u_{jr}{}^m \tag{5.75}$$

where $u_{jr}{}^m$ represents the displacement at nodal point r for j-th mode at time t_m.

On the other hand, the kinematic energy of the bridge $E_j{}^m$ for j-th mode can be written as

$$E_j{}^m = \frac{1}{2} \omega_j{}^2 \sum_i m_i (u_{ji}{}^m)^2 \tag{5.76}$$

where ω_j : angular frequency of j-th mode, and m_j : lumped mass at nodal point i.

Introducing a coordinate $\Gamma_j{}^m$ defined as

$$u_{ji}{}^m = \Gamma_j{}^m \phi_{ji} \tag{5.77}$$

where ϕ_{ji}: amplitude of *j*-th mode at nodal point *i*, and substituting Eq. (5.77) into Eqs. (5.75) and (5.76), one obtains

$$\Delta E_j{}^m = 4\Gamma_j{}^m \sum_r F_r \phi_{jr} \tag{5.78}$$

$$E_j{}^m = \frac{1}{2}\omega_j{}^2 (\Gamma_j{}^m)^2 M_j \tag{5.79}$$

where,

$$M_j = \sum_i m_i \phi_{ji}{}^2 \tag{5.80}$$

Substituting Eq. (5.78) and (5.79) into Eq. (4.?), one obtains the equivalent damping ratio ξ_j for j-th mode as

$$\xi_j = \frac{1}{4\pi} \cdot \frac{\Delta E_j{}^m}{E_j{}^m} = \frac{2}{\pi \omega_j{}^2 \Gamma_j{}^m M_j} \sum_r F_r \phi_{jr} \tag{5.81}$$

Predicted damping ratio vs. amplitude of deck displacement relation determined by Eq. (5.81) is presented in Fig. 5.136. The damping ratios by Eq. (5.81) agree well with the damping ratios determined by Eq. (5.70) based on the numerical decays of free oscillations.

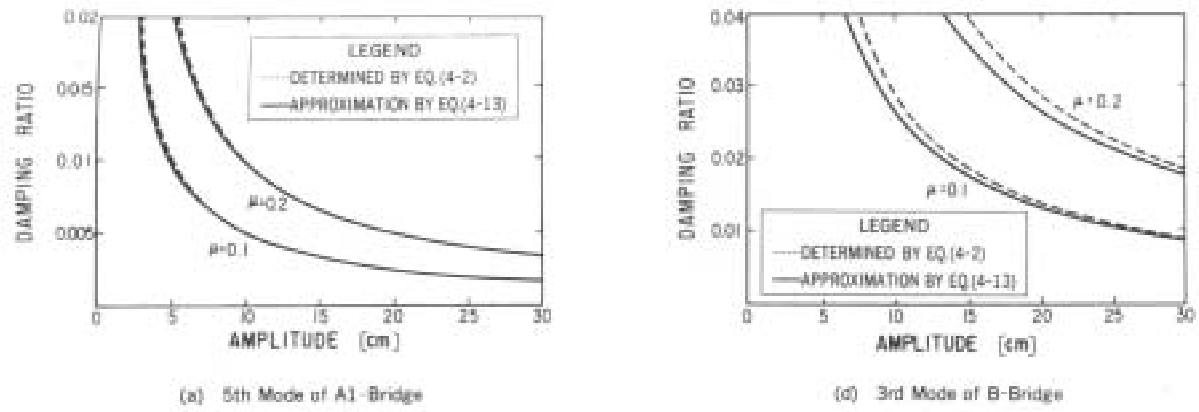

(a) 5th Mode of A-Bridge (b) 3rd Mode of B-Bridge

Fig. 5.136 Damping Ratio vs. Deck Amplitude of Free Oscillation

6) Dependence of Damping Ratios on Mode Shapes

a) Experimental Tests

Damping ratios of cable stayed bridges depend on mode shapes. Since the dependence of damping ratios on mode numbers has not yet been clarified based on measured damping ratios, a free oscillation test for cable stayed bridge models was conducted (Kawashima, Unjoh and Tsunomoto 1991, Kawashima, Unjoh and Tsunomoto 1993). Fig. 5.137 shows the experimental model which was fabricated for simulating the dynamic characteristics of Meiko-nishi Bridge (refer to Fig. 5.115) as prototype. The rigidity and mass of the model was determined assuming the scale of length, density and time equal to 1/150, 1/1 and $1/\sqrt{150}$, respectively. Two supporting conditions of the deck are tested; (1) the deck is supported by only cables as the prototype bridge, and (2) the deck is rigidly fixed to the towers. In the first condition, the prestressed cables which are set in the prototype bridge between the deck and the towers are disregarded in the model bridge because of difficulty involved in modeling the prestressed cables. Eight cable arrangements and the number of cables are considered as shown in Fig. 5.138. The cable type changes from “fan” (Types 3A and 2A) to “harp” (Types 3E and 2C), and the number of cables is either 3 (Type 3A-3E) or 2 (Type 2A-2C). Fig. 5.139 shows the fundamental natural frequencies and natural mode shapes of the models which are predicted by a linear model.

In the free oscillation test, the deck is statically displaced so that the bridge model deforms close to a target mode shape, and then the model is smoothly released to result in a free oscillation. As the target modes, the vertical flexural oscillations and the longitudinal oscillations presented in Fig. 5.139 are considered. Damping ratio is computed from decay of the free oscillation by Eq.(5.61).

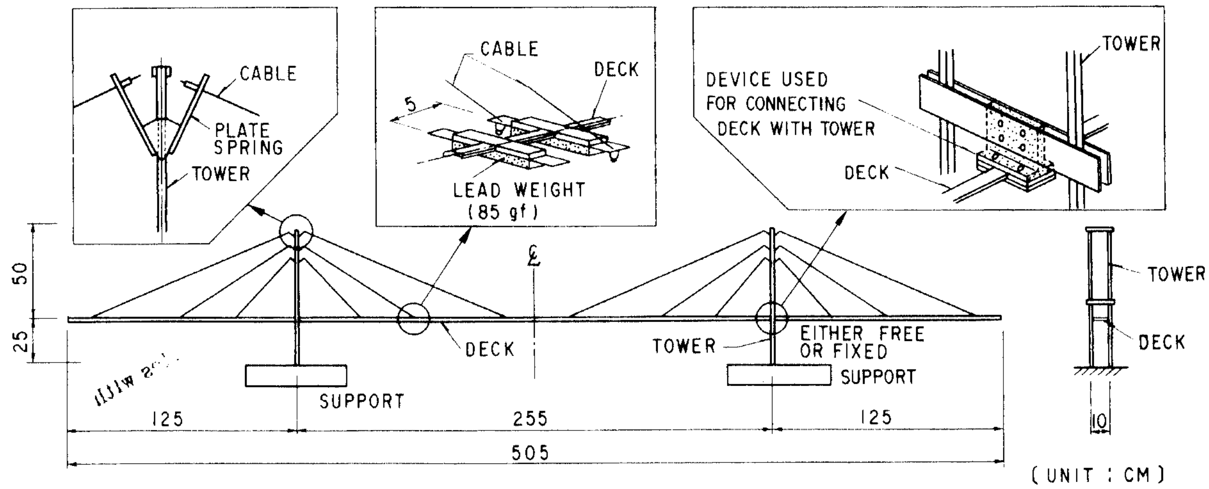

Fig. 5.137 Experimental Model

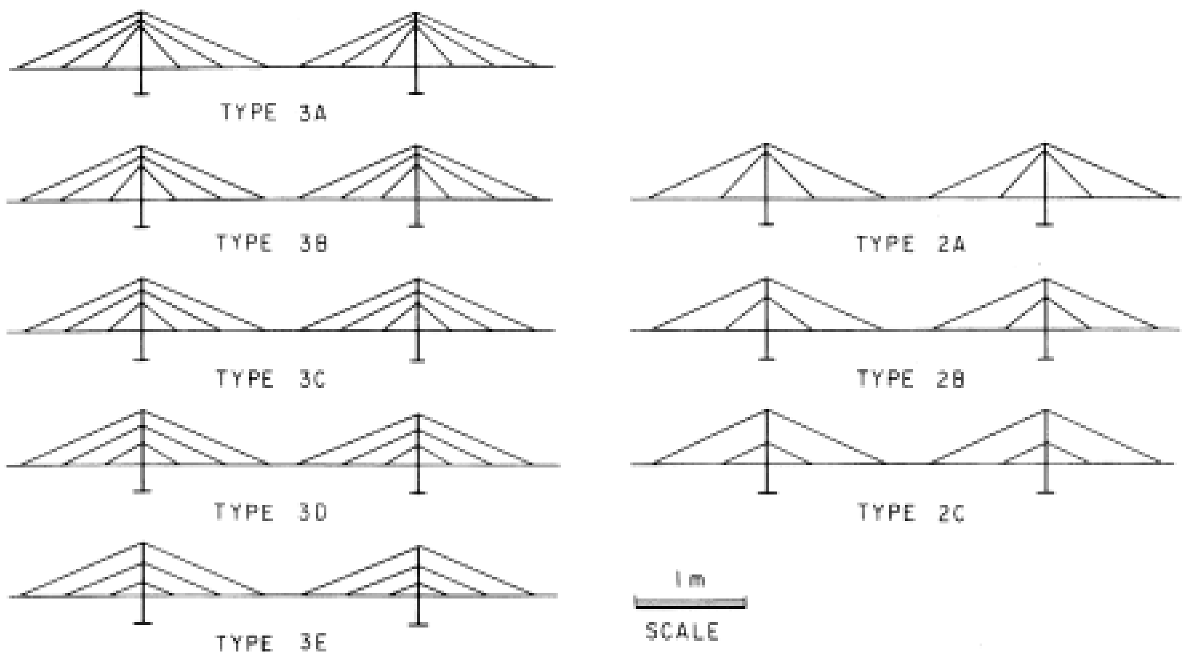

Fig. 5.138 Cable Arrangement

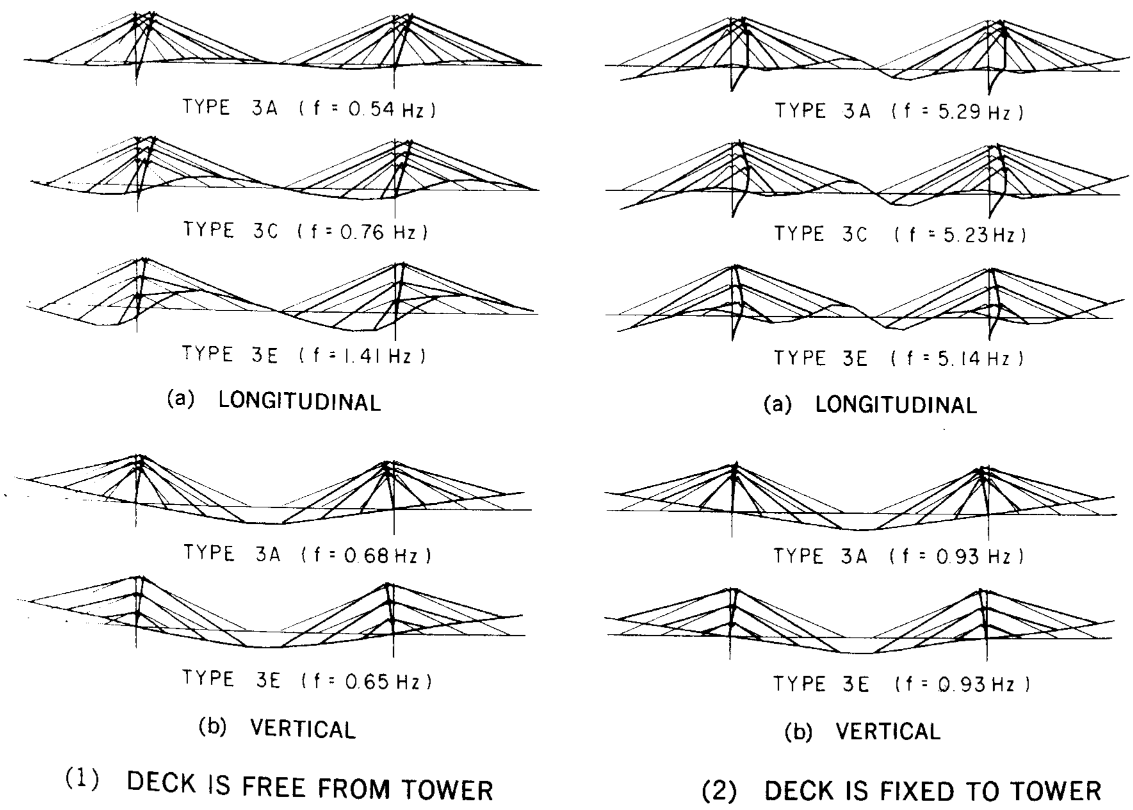

Fig. 5.139 Predicted Mode Shapes

b) Effect of Cable Types on the Damping Ratios in the Longitudinal Oscillation

Fig. 5.140 shows an example of decays of free oscillation when the Type 3A and 3E models are excited in the longitudinal direction. In addition to the cable arrangement, the supporting condition of the deck at the towers is different in this example. Decays of the deck displacement are significantly different between two models showing a dependence of the damping ratios on the cable types and the supporting conditions.

Damping ratios determined by Eq. (5.61) are plotted against oscillation amplitudes in Fig. 5.141. In the longitudinal direction, damping ratios considerably depend not only on the number of cables and the cable types but also on the amplitudes of oscillations. Damping ratios at an amplitude increase as the cable type changes from the fan (Type 3A) to the harp (Type 3E). Such a considerable cable type dependence of the damping ratios results from the flexural deformation of the deck in the vertical direction per unit deck displacement in the longitudinal direction (refer to Fig. 5.139). Larger vertical flexural deformations of the deck dissipatesmore energy resulting in the increase of damping ratios.

The damping ratios also depends on the amplitude of oscillations, and this amplitude dependence of the damping ratios increases as the cable type changes from the fan (Type 3A) to the harp (Type 3E).

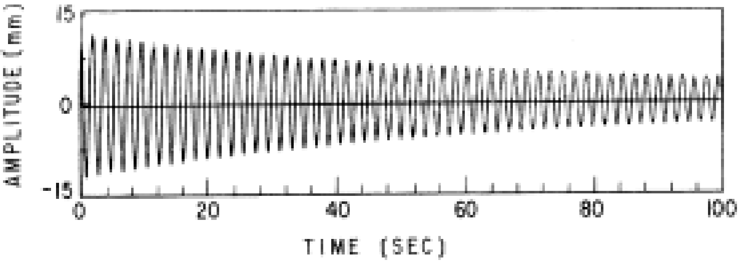

(a) Type 3A, Deck is free from towers

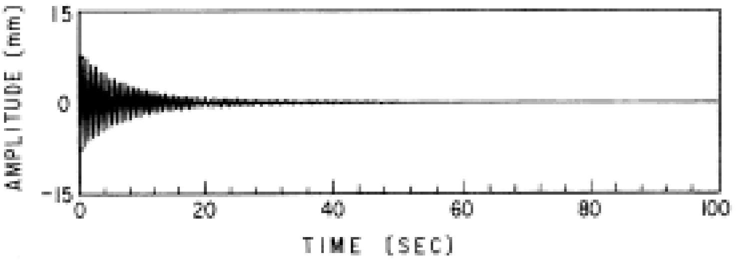

(b) Type 3E, Deck is rigidly connected to towers

Fig. 5.140 Decays of free Oscillations in the Longitudinal Direction

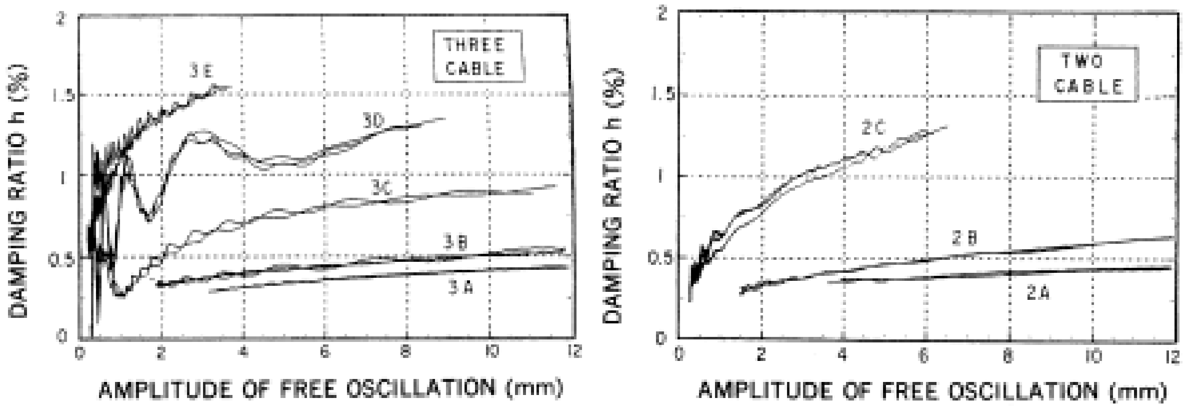

(a) Three Cable Model

(b) Two Cable Model

(1) Deck is free from the tower

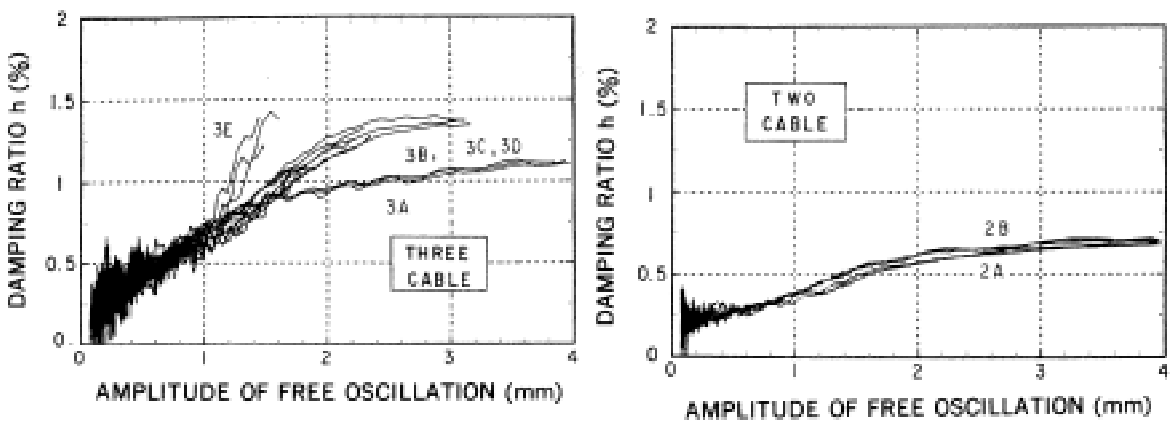

(a) Three Cable Model

(b) Two Cable Model

(2) Deck is connected to the towers

Fig. 5.141 Damping Ratios vs. Oscillation Amplitudes in the Longitudinal Oscillations

c) Effect of Cable Types on the Damping Ratios in the Vertical Oscillation

Fig. 5.142 shows the damping ratios vs. amplitude of oscillations when the model is excited in the vertical flexural modes. Since the supporting condition between the deck and the towers is less sensitive in the vertical flexural oscillations, tests results only for the model bridge with the deckbeing free from the towers are presented here. The damping ratios decrease as the cable type changes from the fan (Type 3A) to the harp (Type 3E). Comparing Fig. 5.142 to Fig. 5.141 (1), the damping ratios for the vertical flexural oscillations are smaller than the damping ratios for longitudinal oscillations. However it is important to note that the damping ratios are the largest in the Type 3A followed by the Type 3B, and Types 3D, 3C and 3E (difference between Types 3D, 3C and 3E is very small. On the other hand, the damping ratios are the largest in the Type 3E and they decrease in the order of Type 3D, 3C, 3B, and 3A in the longitudinal oscillations.

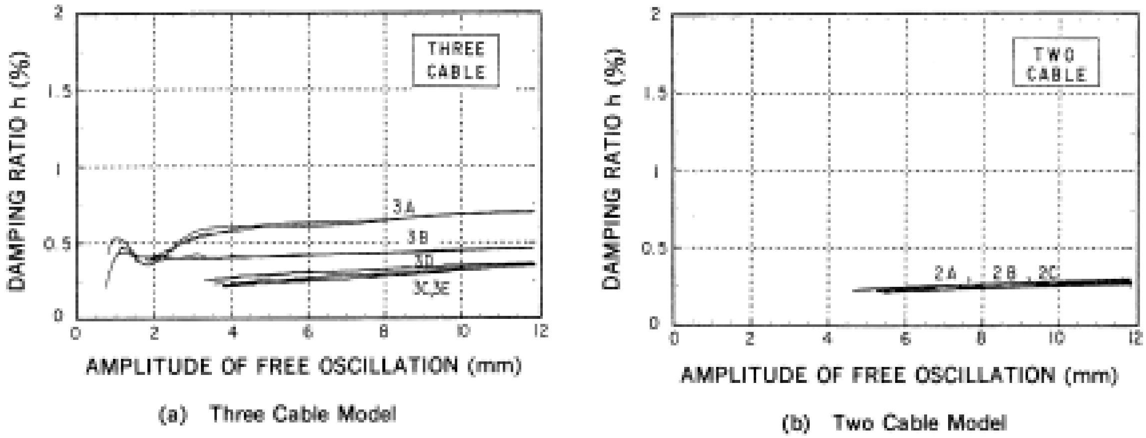

Fig. 5.142 Damping Ratios vs. Oscillation Amplitudes in the vertical Flexural Oscillations (Deck is free from the Towers)

d) Evaluation of Damping Ratios of Cable Stayed Bridges

The method used to evaluate the effect of energy dissipation at movable bearings (Eq. (5.81)) can be extended as follows to evaluate damping ratios of cable stayed bridges.

1) Divide a cable stayed bridge into several structural segments (substructures) in which energy dissipation capability is practically the same.
2) Idealize the *i*-th sub-structure by an n-degree of freedom discrete system, and then evaluate the strain energy of the *i*-th substructure for the *j*-th mode $E_j{}^i$ as

$$E_j{}^i = \frac{1}{2}\sum_k (u_j{}^{ik})^2 k^i u_j{}^{ik} \tag{5.82}$$

where $u_j{}^{ik}$: amplitude at node *k* of *i*-th substructure for *j*-th mode, and k^i: stiffness matrix of *i*-th substructure.

Strain energy of the whole structural system for the *j*-th mode can then be evaluated as

$$E_j = \sum_i E_j{}^i \tag{5.83}$$

3) Determine a relation of the energy dissipation $\delta E_j{}^i$ vs. the strain energy $E_j{}^i$ by Eq. (5.82) in the *i*-th substructure for the *j*-th mode as

$$\delta E_j^{\ i} = f_j^{\ i}(E_j^{\ i}) \tag{5.84}$$

where $f_j^{\ i}$ represents how the energy dissipation $\delta E_j^{\ i}$ develops associated with a deformation in the *i*-th substructure for *j*-th mode with the strain energy $E_j^{\ i}$, and this is called as *energy dissipation function*. Because it is generally difficult to evaluate the energy dissipation function $f_j^{\ i}$ based on numerical analyses, it has to be determined empirically based on appropriate experiments.

In the sub-structures where the energy dissipation function $f_j^{\ i}$ can be represented in terms of displacement at a specific point *k* in the *i*-th substructure for the *j*-th mode $u_j^{\ ik}$, the energy dissipation function $f_j^{\ i}$ may be represented as

$$\delta E_j^{\ i} = f_j^{\ i}(u_j^{\ ik}) \tag{5.85}$$

4) Determine the energy dissipation in the entire structural system δE_j for the *j*-th mode as

$$\delta E_j = \sum_i \delta E_j^{\ i} \tag{5.86}$$

5) Determine the damping ratio of the entire structural system for the j-th mode ξ_j as

$$\xi_j = \frac{\delta E_j}{4\pi E_j} \tag{5.87}$$

e) Evaluation of Energy Dissipation Functions for the Model Bridges

Based on the above procedure, let us determine the energy dissipation functions of the model bridge. Sources of energy dissipation in the model bridge are material nonlinearity of the deck and the towers, and friction at anchors of the cables to the deck and the towers. The towers, the deck and the cable anchors are substructures.

To estimate an energy dissipation function of the tower, the towers are fixed to a test floor as cantilevered beams. A mass each is installed at the top of the cantilevered decks. A simple free oscillation test is conducted for the towers which are being supported as a cantilevered beam. By smoothly releasing the top of the tower from a displaced position, a free oscillation simulating the first mode occurs. Fig. 5.143 shows how damping ratio of the towers depend on the oscillation amplitudes and the mass. As the oscillation amplitudes and the mass increase, the damping ratio of the towers increases. Fig. 5.144 shows the relation between δE_1 and E_1. The relation is nearly independent of the mass, and it is approximated by a least square fit as

$$\delta E_1 = 0.016E_1 + 0.0021E_1^{\ 2} \tag{5.88}$$

Similarly, the energy dissipation functions for the deck and the cable anchor are obtained as

$$\delta E_1 = 0.016 + 0.083E_1^{\ 1.37} \quad \text{(deck)} \tag{5.89}$$

$$\delta E_1 = 0.018\varpi^{2.15} \cdot \theta^2 \qquad \text{(anchor)} \tag{5.90}$$

where θ and ϖ represent angle between the tower and the cable, and angular frequency of the cable oscillation, respectively.

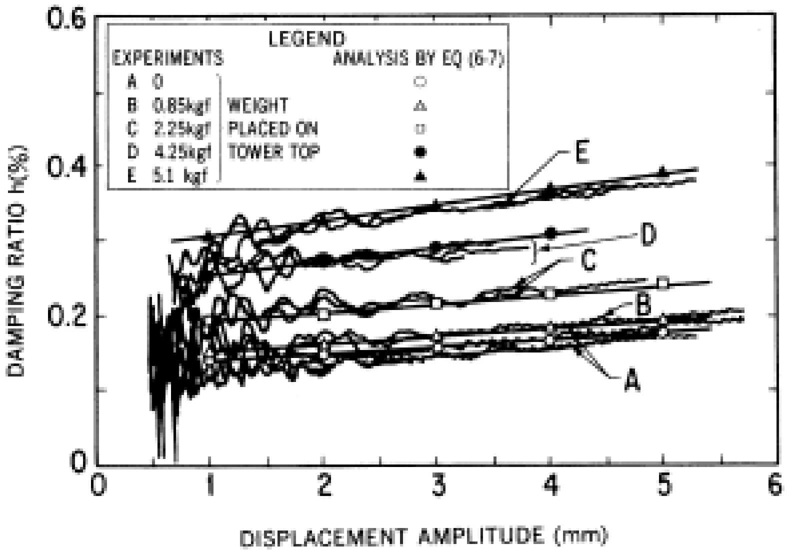

Fig. 5.143 Damping Ratios vs. Oscillation Amplitudes of the Towers

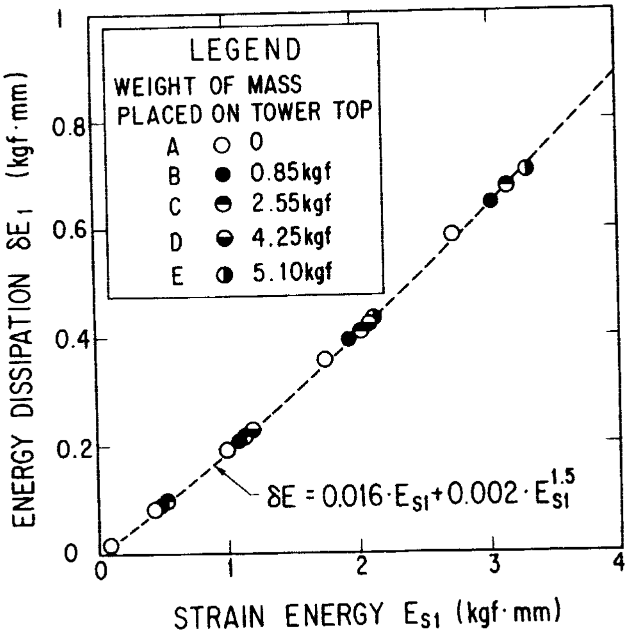

Fig. 5.144 Energy Dissipation vs. Strain Energy of the Towers

f) Evaluation of Damping Ratio of Model Bridges Based on Energy Dissipation Functions

Damping ratios of the model bridge by Eq.(5.87) using the energy dissipation functions of the towers, the deck and the anchors of cables by Eqs.(5.88), (5.89) and (5.90) are shown in Figs. 5.145 and 5.146 for the longitudinal oscillations and the vertical flexural oscillations, respectively. The predicted damping ratios of the model bridge in the longitudinal oscillation increase as the oscillation amplitudes increase and the cable type changes from the fan (type

3A) to the harp (type 3E). Such characteristics agree reasonably well with the experimental results, although the predicted damping ratios are underestimated as the cable type approaches to the harp.

The predicted damping ratios of the model bridge for the vertical flexural oscillations are nearly independent of the cable type. The overall characteristics of the predicted damping ratios are reasonably close to the experimental results. The underestimation of the predicted damping rations may be due to energy dissipation at other than the decks, the towers, and the cable anchorages.

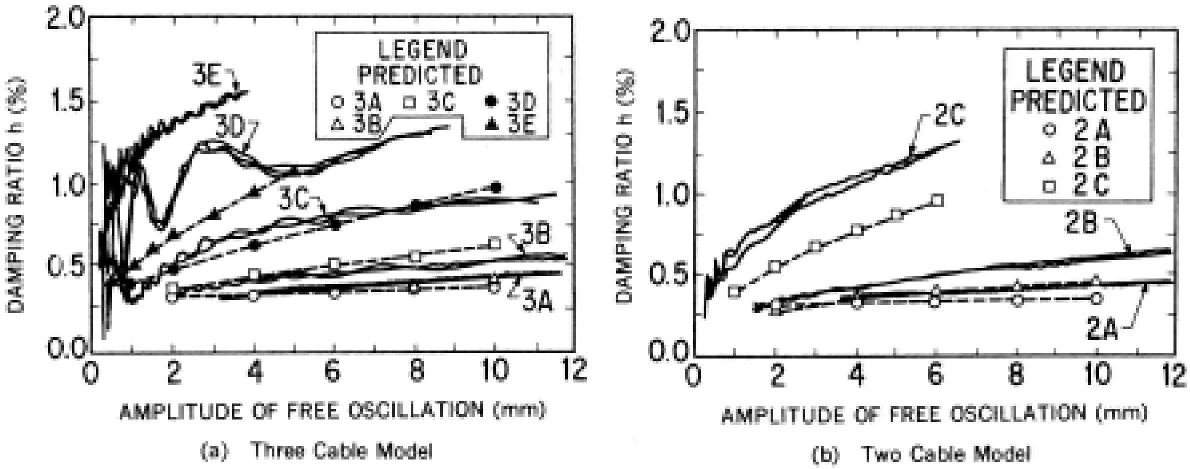

Fig. 5.145 Predicted Damping Ratios vs. Oscillation Amplitudes for Longitudinal Oscillations

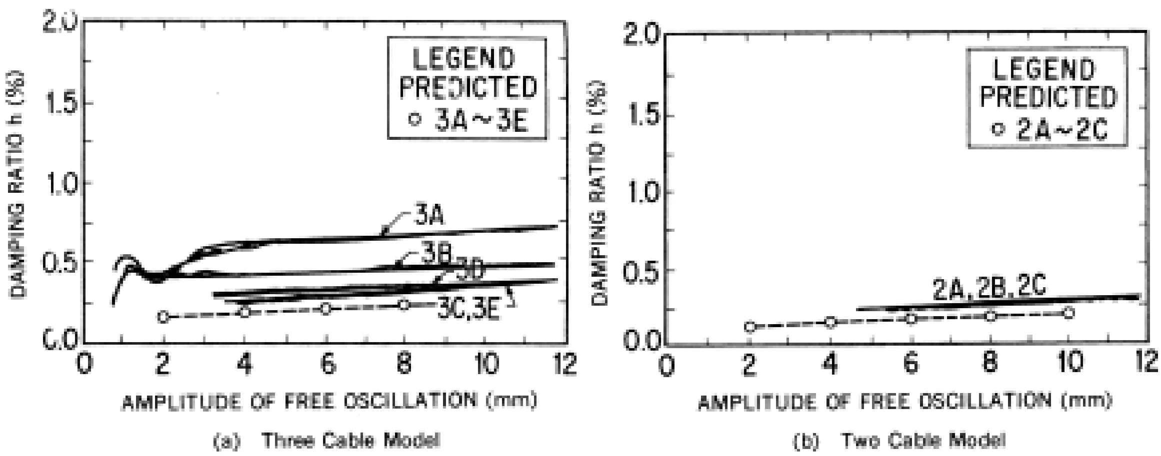

Fig. 5.146 Predicted Damping Ratios vs. Oscillation Amplitudes for Vertical Flexural Oscillations

7) Effect of Propagating Ground Motion for Cable Stayed Bridges

The effect of multiple excitation has been studied for suspension bridges and cable-stayed bridges (Abdel-Ghaffar and Lawrence 1982, Abdel-Ghaffar and Rubin 1983). As an example of such analyses, a seismic response analysis of two cable stayed bridges subjected to multiple excitation, as shown in Fig.147, is presented here (Abdel-Ghaffar 1991). The shorter bridge (model I) consists of a 330 m long center span and two 144 m long side spans, while the longer bridge (model II) has double the span length of model I. They are idealized by continuous beam systems as shown in Fig.147. A nonlinear static analysis is conducted to compute the tangential stiffness of the bridge in its dead-load deformed state, and a linear dynamic response analysis is subsequently performed using this tangential stiffness.

Figs. 148 and 149 show the effect of multiple excitation when the bridges were subjected to array ground accelerations observed during the October 1979 Imperial Valley, California earthquake. In those results, the responses due to dynamic displacements (refer to Eq. (2.11)) as well as the total responses are presented for comparison. It is seen that the multiple support excitation can have a significant effect.

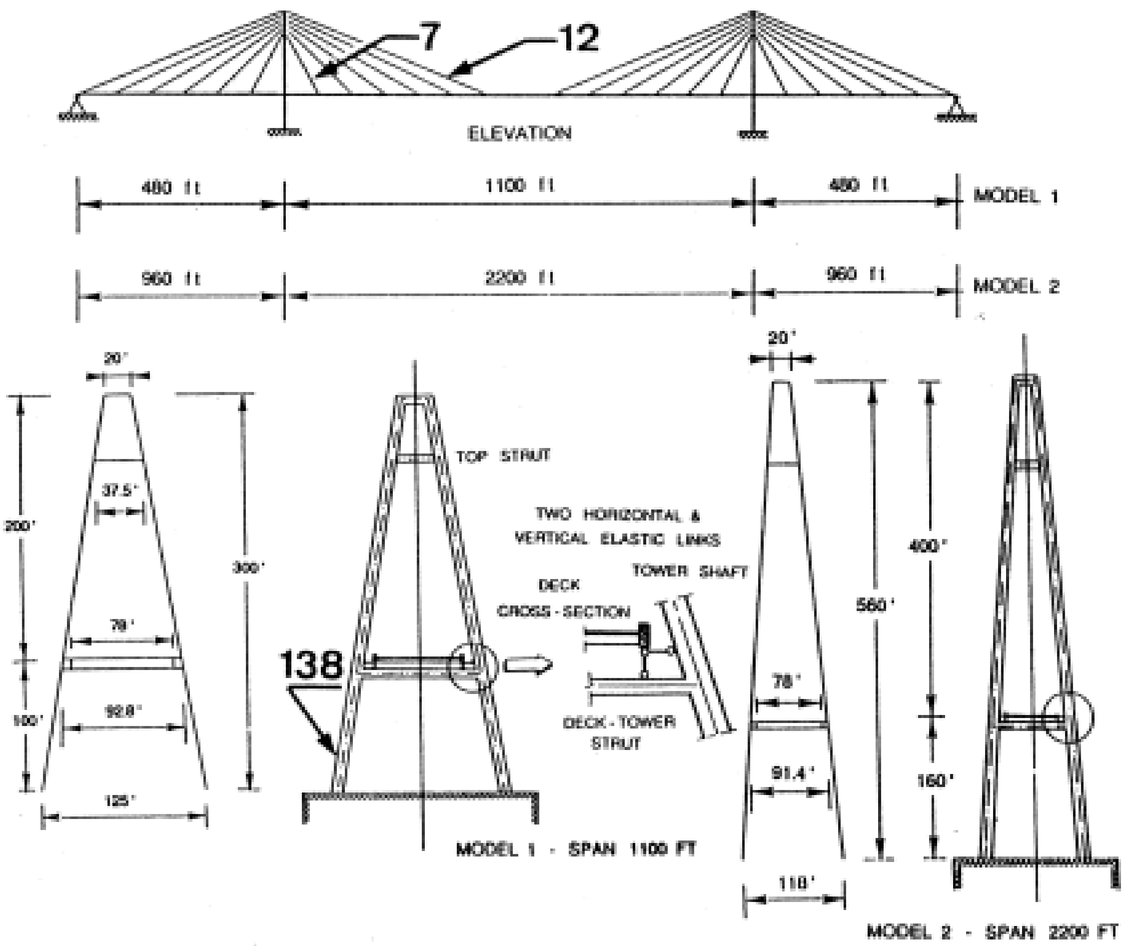

Fig. 5.147 Cable-stayed bridge analyzed

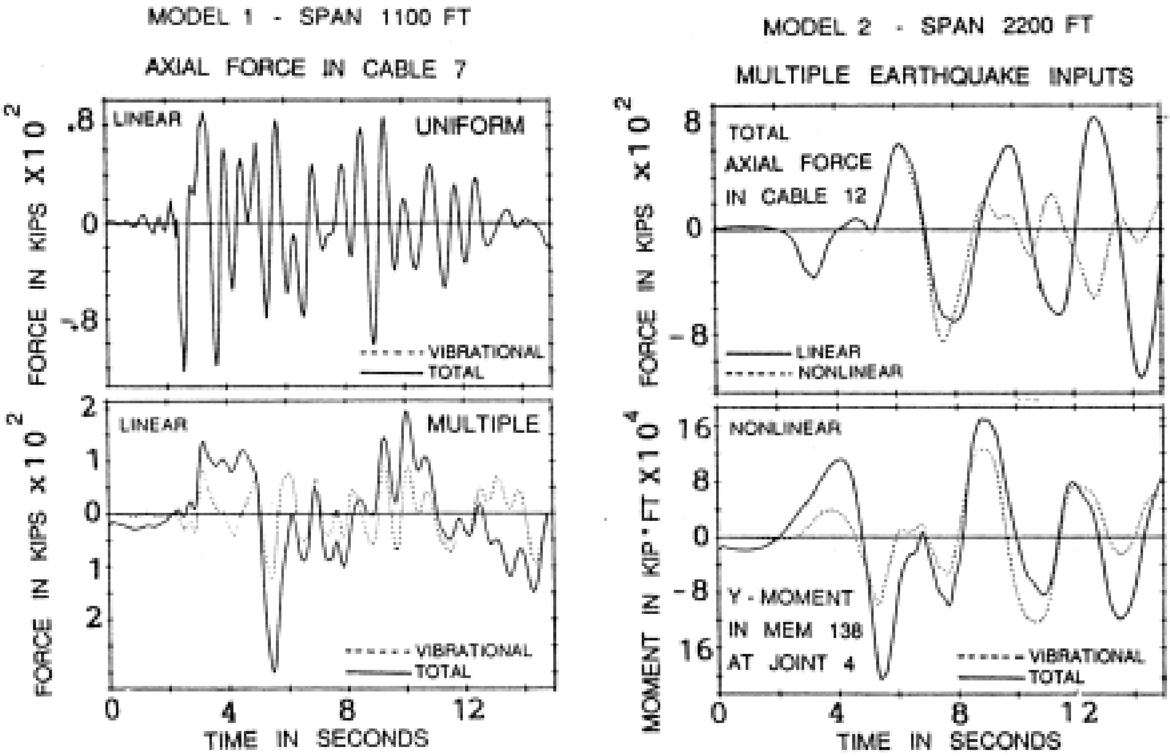

Fig. 5.148 Effect of multiple excitation on the axial force at cable 7

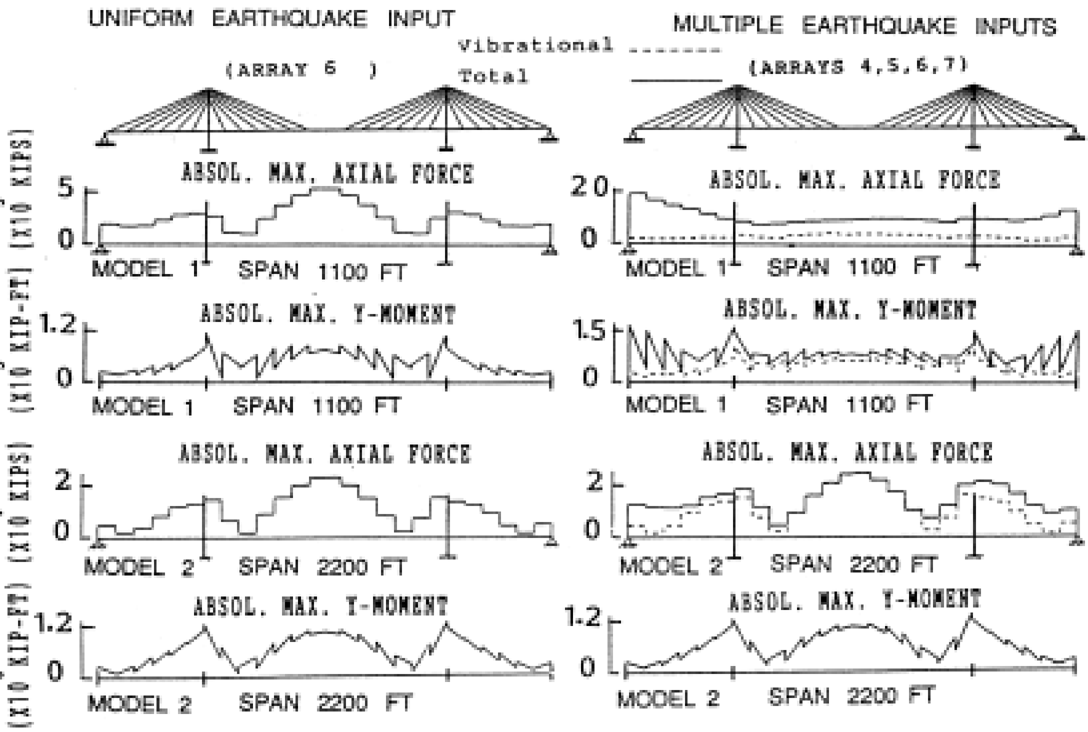

Fig. 5.149 Effect of multiple excitation on the forces at deck

5.12 Seismic Performance of Long-span Bridges during the 1995 Kobe Earthquake

The Akashi Kaikyo Bridge (AK Bridge) is the world longest suspension bridge. It suffered damage in the 1995 Kobe earthquake. When the Kobe earthquake occurred, it was under construction: the abutments and towers were completed, and a part of superstructure was hung by main cables. The fault crossed the bridge between two tower foundations (P2 and P3). This resulted in the permanent movements and rotations in all the abutments and tower foundations. Most predominantly, the P3 tower foundation and A4 abutment were dislocated 1.3 m and 1.4 m, respectively, relative to the 1A abutment and 2P tower foundation. as shown in Fig. 150. This resulted in the increase of center span length from originally designed 1990m to 1990.8 m and the total length from 3910m to 3911.09 m. Permanent lateral drift of 0.15m and 0.1m occurred at the top of tower 1 and tower 2, respectively, due to permanent rotation as well as the lateral offset. A settlement of about 20 mm was found in the P2 tower foundation. However, an examination after the earthquake showed that such a permanent drift brought minor effect to the stability and safety of the AK bridge because the strain was minor due to the long span (Saeki et al, 1997; Yasuda et al, 2000). Fault traces were known based on a geotechnical survey at the preliminary design stage, and it was reflected in the determination of the locations of foundations because soil near a fault is generally weak.

Since the AK Bridge was party instrumented from the construction stage, several important records were obtained in the Kobe earthquake. Most important record was measured at the top and mid-height of P2 tower by velocity sensors. Fig. 151 shows the locations of sensors and velocity response at the top of P2. The peak velocity was about 1.3 m/s and 0.9 m/s in transverse and longitudinal directions, respectively The predominant frequencies of the velocity response were 0.47Hz and 0.40Hz in longitudinal and transverse directions, respectively. Long response with a duration over 180 seconds was induced, which may be attributed to low damping of the tower. Peak acceleration computed from the velocity was over l g in transverse direction.

Based on the measured response, two analyses were conducted; first was to a simulation of the response of the tower in the H-k-n earthquake, and the second was an evaluation of the seismic safety of the completed bridge subjected to the near-field ground motion. In the response evaluation of the tower in the H-k-n earthquake, the tower, the foundation and soils were idealized by a two dimensional finite elementa and beams. Effect of cables was idealized by lumping the tributary mass of cables at the top of tower. The ground acceleration measured at the Kobe Observatory of Japan Metheorological Agency during the 1995 Kobe Earthquake was used as an input ground motion. The JMA Kobe Observatory is about 15km from the AK Bridge. The acceleration at 330 m deep bedrock with shear wave velocity of 880 m/s was computed from the JMA Kobe record, and it was applied at the surface of Kobe Layer with shear wave velocity of 880 m/s to compute the ground motion at the granite bedrock with shear wave velocity of 2,000 m/s. (Morikawa et al, 1 998; Ninomiya et al, 2000; Yasuda et al, 2000). The granite bedrock motion was then applied at the 268m deep bedrock to compute the soil, P2 foundation and P2 tower response.

Fig. 152 shows the comparison of measured and computed response velocity at the top of P2 tower. Accuracy of the numerical simulation is poor, It may be attributed to at least following reasons.

- The input ground motion measured at JMA Kobe Observatory was not close enough to the AK Bridge. Hence, numerical calculation of ground motion at the construction site from the JMA Kobe record includes tremendous error.
- Multiple excitation and spatial variation of ground motion were disregarded.
- Effect of constraint of tower by cables was idealized by only lumping the tributary mass

of cables at the top of tower.

- Rupture process of the fault was not considered.

The same ground motion was used to compute the response of the total bridge system so as to evaluate the safety of the completed bridge. Main interest was to know whether the AK Bridge was safe or not if it had been completed when the earthquake occurred. Figure 5 shows steel stress at corner induced at the bottom ofP2 and P3 towers. The peak stress was 434 MPa and 430 MPa at P2 and P3 towers, respectively. Since it was less than the yield stress of 451MPa, it was decided that the AK Bridge was safe even if the completed bridge was exposed to the H-k-n earthquake (Saeki et al, 1997). The AK Bridge was completed and put in service in April 1998.

References

Abdel-Ghaffar, A.M. and Lawrence, I.R. (1982), “Suspension bridge response to multiple-support excitations,” Journal of Engineering Mechanics Division, ASCE, 108(2), 419-435

Abdel-Ghaffar, A.M. and Rubin, L. (1983), “Lateral earthquake response of suspension bridges,” Journal of Structural Division, ASCE, 109(3), 664-675

Abdel-Ghaffar, A.M. (1991), “Cable-stayed bridge under seismic action,” Cable-Stayed Bridges-Recent Developments and Their Future, Edited by Ito, M. et al, Elsevier, 171-192

Chang, K.C., Tsai, D.W. and Sung, Y.C. (2000), “Seismic performance of highway bridges,” Earthquake Engineering and Engineering Seismology, 2(1), 55-77.

Chen, M.C., and enzien, J. (1975), “Analytical investigations of seismic response of short, single or multiple-span highway bridges,” Report No. UCB/EERC 75-4, Earthquake Engineering Research Center, University of California, Berkeley, USA

Ghasemi, H., Yen, P. and Cooper, J.D., (2000), “The 1999 Turkish earthquakes: post earthquake investigation of structures on the trans European motorway,” 2nd International Workshop on Mitigation of Seismic Effects on Transportation Structures (Edited by Loh, C. H. et al), 337-348, National Center for Research on Earthquake Engineering, Taipei, Taiwan

Goldsmith, W. (1960), “Impact,” Edward Arnold, London

Hardin, B. O. and Drnevich, V, P. (1972), “Shear Modulus and Damping in Soils, Design Equation and Curves, Journal of Soil Mechanics and Foundation Engineering, ASCE, 98(7), 667-692, USA.

Ito, R., Kosa, K., Ito, R., and Sakamoto, M. (1998), “Lateral Deformation Capacities of Pile Foundations,” Journal of Structural Engineering, JSCE, 39A, 1835-1394.

Iwasaki, T., Kawashima, K., Takagi, Y. and Aizawa, K. (1980), “Dynamic soil-structure interaction analysis of Kaihoku bridge,” Proc. JSCE, 322, 15-24

Japan Road Association (1996), Design Specifications of Highway Bridges, Maruzen Publishing Co. Ltd, Tokyo, Japan

Kawashima, K. and Penzien, J. (1976), “Correlative investigations on theoretical and experimental dynamic behavior of a model bridge structure,” Report No. EERC 76-26, Earthquake Engineering Research Center, University of California, Berkeley, USA

Kawashima, K. and Penzien, J. (1979), “Theoretical and experimental dynamic behavior of a curved model bridge structure,” Earthquake Engineering and Structural Dynamics, 7, 129-145

Kawashima, K., Unjoh, S., and Azuta, Y. (1988), “Damping characteristics of cable-stayed bridges,” Proc. 9th WCEE, 471-476, Tokyo/Kyoto, Japan

Kawashima, K. and Unjoh, S. (1989), “Damping characteristics of cable stayed bridges

associated with energy dissipation at movable supports," Proc. JSCE, Structural Engineering and Earthquake Engineering, 6-1, 123-130
Kawashima, K., Unjoh, S., and Azuta, Y. (1990), "Analysis of damping characteristics of a cable stayed bridge based on strong motion re cords," Proc. JSCE, Structural Engineering and Earthquake Engineering, 7-1, 169-178
Kawashima, K., Unjoh, S., and Tsunomoto, M. (1993), "Estimation of damping ratio of cable-stayed bridges fopr seismic design," Journal of Structural Engineering, 119-4, 1015-1031, ASCE
Kawashima, K. and Mizoguchi, A. (2000), "Seismic response of a reinforced concrete arch bridge," Proc. 12 WCEE, Paper No. 1824 (CD-ROM), Auckland, New Zealand
Kawashima, K. and Watanabe, G. (2001), "Analysis of pounding of two elastic rods using impact spring element," Structural Engineering and Earthquake Engineering, 675/I-55, Proc. JSCE, 125-139
Kawashima, K. and Hosoiri, K. (2002), "Effect of Nonlinear Rocking Response of Direct Foundations on the Hysteretic Behavior of Bridges," Proc. JSCE, Structural Engineering and Earthquake Engineering, 703/I-59, 97-111.
Kawashima, K., Uehara, K., Shoji, G. and Hoshi, S. (2002), "Shaking table test and analysis of a model bridge for identifying the effect of pounding and restrainers," Proc. JSCE, Structural Engineering and Earthquake Engineering, 703/I-59, 221-236
Liu, W.D., Riedes, J.M., Imbsen, R.A., Priestley, M.J.N., and Seible, F. (1990), "Response of a major highway bridge during the Whitter earthquake," Proc. 4th US National Conference on Earthquake Engineering, USA
Monti, G., Nutti, C., Pinto, P. and Vanzi, I. (1994), "Effects of non-synchronbous seismic input on the seismic response of bridges," Proc. 2nd International Workshop on Seismic Design and Retrofit of Reinforced Concrete Bridges, Edited by Park, R., 95-112, Queenstown, New Zealand
Penzien, J., Scheffey, C. F. and Parmelee, R. A. (1964), "Seismic analyses of bridges on long piles," Proc. ASCE, Vol. 90, EM 3, 223-254, USA.
Priestley, M.J.N., Seible, F. and Calvi, G.M. (1996), "Seismic design and retrofit of bridges," John Wiley & Sons, Inc., New York, USA.
Saeki, S., Kurihara, T., Toriumi, R. and Nishitani, M. (1997), "Effect of the Hyogoken nanbu earthquake on the Akashi kaikyo bridge," Proc. 2nd Italy-Japan Workshop on Seismic Design and Retrofit of Bridges, Rome, ItalySchnable, P. B., Lysmer, J. and Seed, H. B. (1972), SHAKE-A Computer Program for Earthquake Response Analysis of Horizontally Layered Sites, EERC 72-12, University of California, Berkeley, CA, USA.
Somaini, D.R. (1987), "Seismic behavior of girder bridges for horizontally propagating waves," Earthquake Engineering and Structural Dynamics, 15, 777-793
Takeda, T., Sozen, M. and Nielsen, N. (1970), Reinforced Concrete Response to Simulated Earthquakes, Journal of Structural Engineering, Div. ASCE, 96(12), 2557-2573.
Teng, W.S. and Penzien, J. (1973), "Analytical investigations of the seismic response of long multiple span highway bridges," Report No. EERC 73-12, Earthquake Engineering Research Center, University of California, Berkeley, USA
Tseng, W.S. and Penzien, J. (1975), "Seismic analysis of long multi-span highway bridges," Earthquake Engineering and Structural Dynamics, 4, 25-48.
Watanabe, G. and Kawashima, K. (2001), "Effectiveness of cable-restrainers for mitigating rotation of a skewed bridge subjected to strong ground shaking," Proc. JSCE, Structural Engineering and Earthquake Engineering, 675/I-55, 141-159
Werner, S.D., Lee, L.C., Wong, H.L. and Trifunac, M.D. (1979), "Structural response to traveling seismic waves," Journal of Structural Division, ASCE, 105(12), 2547-2654
Williams, D. and Godden, W. (1979), "Seismic response control of long curved bridge

structures: Experimental model studies," Earthquake Engineering and Structural Dynamics, 7, 107-128

Yabe, M. and Kawashima, K. (1999), "Effect of the yield strength ratio between the column and pile foundation on the plastic deformation of pile foundation," Journal of Structural Mechanics and Earthquake Engineering, JSCE, 626(I-48), 51-68, Tokyo, Japan

Yabe, M. (2000), "Investigation on seismic design method of bridge-pile systems," Ph. D. Dissertation submitted to Tokyo Institute of Technology.

Yabe, M. and Kawashima, K. (2000), "Hysteretic response of pile foundations subjected to near-field ground motions," Proc. 2nd International Workshop on Mitigation of Seismic Effects on Transportation Structures, 246-257, Edited by Loh, C.H. et al, Taipei, Taiwan

Yasuda, M., Kitagawa, M. Toriumi, T. and Fukunaga, S. (2000), "Seismic design and behavior during the Hyogoken nanbu earthquake of the Akashi kaikyo bridge," Proc. 12th WCEE, Auckland, New Zealand